

**Experimental Cardiovascular Imaging (ExCaVI)**

**Core Facility Small Animal Imaging**

**Head: Prof. Dr. rer. nat. Volker Rasche**

**Department of Internal Medicine II**

**University of Ulm**

**High-resolution Magnetic Resonance  
Imaging analysis of breast cancer xenograft  
on the chick chorioallantoic membrane**

Dissertation applying for

Doctor Degree of Medicine (Dr. med.)

Faculty of Medicine, University of Ulm

Presented by

Zhi Zuo

Born in Lian' shui, P. R. China

2015

Amtierender Dekan: Prof. Dr. Thomas Wirth

1. Berichterstatter: Prof. Dr. Volker Rasche

2. Berichterstatter: Prof. Dr. Thomas Simmet

**Tag der Promotion: 19. 11. 2015**

## Contents

Contents .....	I
Abbreviations .....	III
1 Introduction.....	1
1.1 Chicken embryo model and chorioallantoic membrane (CAM) system.....	1
1.2 Main application of CAM model in current researches .....	2
1.3 Magnetic Resonance Imaging of the CAM model.....	4
1.3.1 Magnetic resonance imaging .....	4
1.3.2 Limitation of CAM model for MRI research and corresponding solutions .....	5
1.3.3 Investigated MRI techniques .....	6
1.4 Objective of the thesis .....	11
2 Materials and Methods.....	12
2.1 Materials .....	12
2.1.1 Fertilized Eggs .....	12
2.1.2 Cells .....	12
2.1.3 Laboratory Equipments.....	12
2.1.4 Analysis Software .....	12
2.1.5 Consumable Items.....	13
2.2 Chicken Embryos .....	13
2.3 Immobilization protocol optimization.....	14
2.3.1 Cooling Regime Optimization .....	14
2.3.2 Immobilization using anesthetics.....	15
2.3.3 Anesthetics application combined with pre-cooling.....	16
2.3.4 Assessment Criteria.....	16
2.4 Cancer Cell Grafting.....	16
2.5 In Ovo MRI .....	17
2.5.1 MR Unit .....	17
2.5.2 Tumor growth monitor.....	17
2.5.3 DWI and T <sub>2</sub> mapping .....	19
2.5.4 Gadolinium contrast agent assessment in CAM model .....	19
2.5.5 USPIO (Feraspin <sup>TM</sup> XS) bio-distribution assessment in ovo.....	26
2.6 Statistical Analysis .....	26
3 Results.....	27
3.1 Immobilization protocol.....	27
3.1.1 Novel cooling regime.....	27
3.1.2 Immobilization with anesthetics .....	28
3.1.3 Isoflurane application combined with pre-cooling .....	29
3.2 High resolution T <sub>2</sub> -weighted embryo anatomical MR analysis .....	29
3.3 Tumor growth monitoring .....	31
3.4 Histological workup of breast cancer cell xenograft.....	35
3.5 T <sub>2</sub> maps and DWI analysis of tumor on CAM .....	36
3.6 MR contrast agent assessment with CAM model.....	38

CONTENTS	II
3.6.1 Gadolinium CA assessment .....	38
3.6.2 USPIO (Feraspin <sup>TM</sup> XS) bio-distribution assessment in ovo .....	47
4 Discussion .....	49
4.1 CAM model – an alternative option for cancer xenograft research .....	49
4.2 MRI imaging for CAM model.....	52
4.2.1 Assessment of the morphology of chicken embryos and cancer cell xenografts on the CAM.....	52
4.2.2 T <sub>2</sub> mapping and DWI application on CAM model .....	52
4.2.3 CA assessment in CAM system.....	53
5 Summary .....	58
6 Reference .....	60
7 Acknowledgments.....	69
8 Curriculum vitae .....	71

**Abbreviations**

ADC	Apparent diffusion coefficient
BG	Background
CA	Contrast agent
CAM	Chorioallantoic membrane
CE	Contrast agent enhanced
cHSA	cationized human serum albumin
CNS	Central Nervous System
DMSO	Dimethylsulfoxide
DOX	Doxorubicin
DOTA	1,4,7,10-tetraazacyclododecane-1,4,7,10-tetraacetic acid
DTPA	Diethylene triamine pentaacetic acid
DWI	Diffusion weighted imaging
EDTA	Ethylenediaminetetraacetic acid
EMCH	Eoxorubicin-6-maleimidocaproyl hydrazone
FLASH	Fast Low Angle Shot
Gd	Gadolinium
GRE	Gradient echo
HH	Hamburger and Hamilton
HSA	Human serum albumin
MR	Magnetic resonance
MRA	Magnetic Resonance Angiography
MRI	Magnetic resonance imaging
NHS	N-hydroxysuccinimide
NSA	Number of signals averaged or added
PbP	Protein based polypeptide copolymer
PEO	Polyethylene oxide
RARE	Rapid acquisition with relaxation enhancement
RES	Reticuloendothelial system
RF	Radiofrequency
ROI	Regions of interest
SE	Spin echo
SNR	Signal to noise ratio
stddev	Standard deviation
T <sub>1</sub>	Spin-lattice relaxation
T <sub>2</sub>	Spin-spin relaxation
TA	Acquisition Time
TE	Echo Time
TR	Repetition Time
UC	Urethane/ $\alpha$ -chloralose
USPIO	Ultra small-sized superparamagnetic iron oxide

## 1 Introduction

### 1.1 Chicken embryo model and chorioallantoic membrane (CAM) system

In vivo models play a crucial role in basic and medical research. Progress in many fields like regenerative medicine, cancer research, infection biology, and drug discovery is strongly dependent on in vivo models to transfer in vitro results and to develop new therapeutic approaches (Strome and Doudet 2007; Morgan et al. 2000; Wang et al. 2002).

Among all kinds of in vivo models, the chicken embryo model occupies a unique and important position with the physical structure of the chorioallantoic membrane. Chicken embryo development lasts 21 days before hatching. Hamburger and

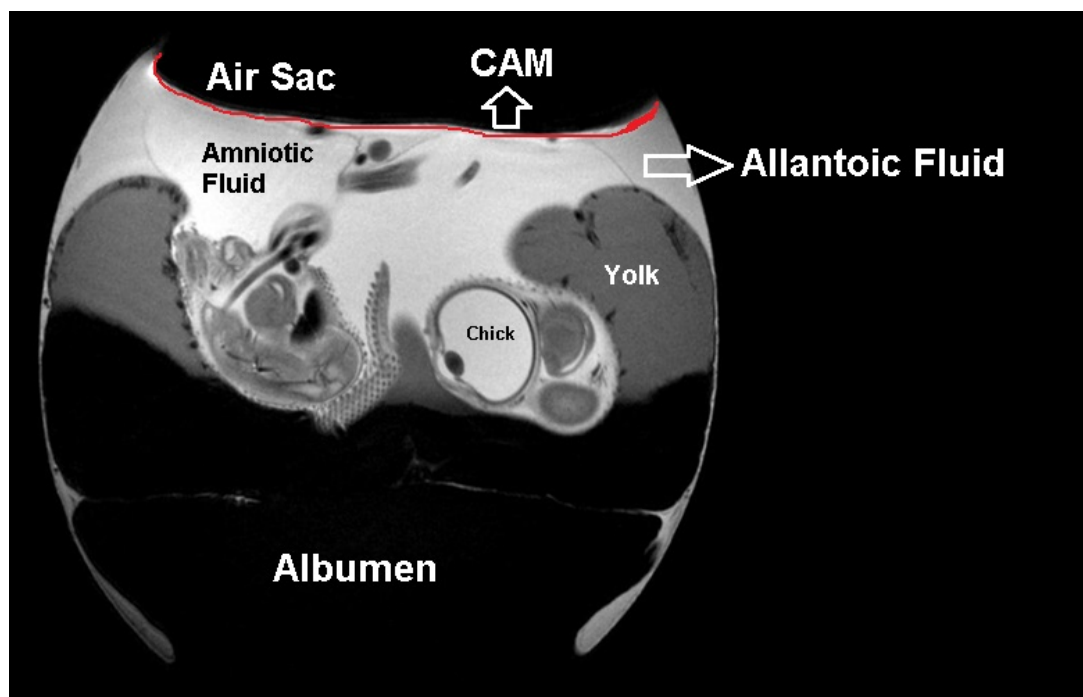


**Figure 1:** The in ovo structures and CAM (chorioallantoic membrane) system. Magnetic Resonance image of in ovo structure of chick embryo at 10th day of incubation, CAM is marked. Hamilton classified the embryo development depending on a series of stages designed based on the external characteristics of the embryo (Hamburger and Hamilton 1951). The 21 days incubation period corresponds to 46 stages, known as the HH (Hamburger and Hamilton) stages.

The chick chorioallantoic membrane is the transparent outermost extraembryonic

membrane lining the no cellular eggshell membrane (Figure 1), which is the respiration organ of chicken embryos. It is attached to the embryo, and also connected to the embryonic blood circulation by the allantoic arteries and veins. CAM is generated by fusion of the splanchnic mesoderm of the allantois and the somatic mesoderm of the chorion during day 4-5 of incubation. The fused CAM grows and covers the entire surface of the inner egg shell membrane by day 12 of incubation. Except the cover range and size, other features of CAM also change during embryo development, such as the composition of the extracellular matrix, the degree of differentiation of both endothelial cells and vessels, the characteristics of the inter-endothelial junctions, as well as the location of the vessels within the CAM (Ribatti et al. 2001). Rapid capillary proliferation in CAM continues until day 11 of incubation. The mitotic index then dramatically decreases and growth rate stays minimal. The vascular system attains its final arrangement on day 18 of incubation, just before hatching. The CAM is important for chicken embryos. It serves as a necessary support for all the extraembryonic arteries, veins, and respiratory capillaries. At the same time it forms part of the wall of the allantoic sac, which contains allantoic fluid, collecting soluble, insoluble and gaseous excretory products, and increasing in size as the embryo develops. Most important, it transports oxygen from the air sac, electrolyte (sodium and chloride) from the allantoic sac, and also calcium from the eggshell for bone mineralization into the embryonic vasculatures.

## **1.2 Main application of CAM model in current researches**

Actually for this special in vivo model there has been a long history for research application. The first preserved report of a detailed description of the chick embryo is credited to Aristotle (384–322 BC), a Greek philosopher (Aristotle 1970). Until today the CAM system remains widely been used in developmental biology, gene expression analysis, stem cell (Glover et al. 2009), infection research (Härtl et al. 2004), cardiovascular research (Le Noble et al. 1993; Taber, Keller, and Clark 1992; Higgins and Pappano 1981), and also as a bioreactor (Zhu et al. 2005).

The CAM system is also successfully used to study cancer invasion and metastasis (Armstrong, Quigley, and Sidebottom 1982; Koop et al. 1995), progression and its pharmacological treatment (Morad et al. 2011; Morad et al. 2013; Büchele et al. 2006; Syrovets et al. 2005; Vogler et al. 2008; Estrada et al. 2010), neovascularization of heterologous normal and neoplastic implants (Kaufman et al. 1956), proliferative response of blood vessels to tumor angiogenesis factors (Loos et al. 2014), pharmacokinetics (Büchele et al. 2005), properties of novel nanomaterials (Loos et al. 2014; Lunov et al. 2011), or as a model system to study microsurgical instruments and techniques (Leng et al. 2004).

Although the nude murine model is still the golden standard as *in vivo* xenotransplantation tumor model, the CAM system offers various advantages (Table 1) compared to xenograft murine tumor models. First of all, the full development of the lymphoid system does not happen before the very late stage of incubation. Hence the chick embryo model is a naturally immune-deficient host allowing xenotransplantation of many kinds of tumors (Janse and Jeurissen 1991) without species-specific limitations. In addition, the blood vessel network of the CAM provides an excellent environment for primary tumor formation with organoid structures and a basis for angiogenic blood vessel formation (Deryugina and Quigley 2008). According to European law (Directive 2010/63/EU of the European Parliament and of the Council of 22 September 2010 on the protection of animals used for scientific purposes), the CAM system represents an intermediate stage between isolated cultured cells and animals, which does not raise any ethical or legal concerns, thus being an attractive replacement for *in vivo* animal experiments. Chicken eggs are available year-round, they are inexpensive, and they can be purchased in any specified quantity. Chicken eggs can be incubated to any stage of interest thus simplifying experimental design. Considering the obvious advantages, it forms an excellent platform for exploratory biomedical research.



Table 1: comparison between CAM (chorioallantoic membrane) and Mammalian models for cancer cell implantation

Chick embryo CAM model	Mammalian Models
Low cost	High cost
In vivo model	In vivo animal model
Operation is simple to implant cancer cells	Operation is more complex
Direct visualization through shell window	Direct visualization not allowed
Short cell implantation time	Longer implantation time
Tissue and blood sampling is easy to be finished but sample amount is limited	Tissue and blood sampling requires more invasive procedures but larger quantity
Cost-effective model for utilization of expensive and limited reagents (e.g., cytokines, antibodies)	Cost-ineffective model

### 1.3 Magnetic Resonance Imaging of the CAM model

#### 1.3.1 Magnetic resonance imaging

Magnetic resonance imaging (MRI) provides high resolution, in-depth anatomical images without the use of ionizing radiation. MRI is based on the monitoring of the distribution of  $^1\text{H}$  protons. MRI typically depicts the content and interactions of water in tissues with cellular constituents such as proteins, carbohydrates, and electrolytes. MRI is also used to monitor proton density, as well as diffusion processes. It is a powerful technique for non-invasive diagnosis of the anatomy, physiology, and pathophysiology on the basis of superior spatial resolution and contrast which is useful in providing both anatomical and functional images, among which cancer diagnosis is one of the paramount applications for MRI.

Early cancer detection is a major factor in the reduction of mortality and cancer management cost. MRI is the method-of-choice for noninvasive assessment of tumors, having an essential role in classification, grading, follow-up and therapeutic management, due to its soft tissue resolution, safety and diversity. MRI can provide structural, biochemical and functional information regarding the tumor and its surrounding parenchyma. In the last few years, a broad range of MRI techniques have been developed to provide feedback and surrogate markers for therapeutic

response including tumor blood volume, perfusion, vessel permeability, oxygenation and vessel size (Gerstner et al. 2008).

### 1.3.2 Limitation of CAM model for MRI research and corresponding solutions

Despite the obvious advantages and wide acceptance of both MRI and CAM model, the application of MRI for analysis of cancer xenograft on CAM has not been investigated. So far the application of in ovo MRI was limited to monitoring the growth of the main organs of embryos, such as brain (Peebles et al. 2003), heart (Holmes et al. 2008; Holmes et al. 2009), liver (Bain et al. 2007), eyes (Goodall, Kisiswa, Prashar, Faulkner, Tokarczuk, Singh, Jonathan T. Erichsen, et al. 2009), limbs (Xu et al. 2012), and the germinal disc (Burkhardt et al. 2011).

The application of MRI for the analysis of the tumor in ovo has been limited by motion of the embryo, causing severe motion artifacts, which do not allow detailed visualization and assessment of small solid tumor tissues on the CAM.

Early immobilization methods for chick embryo MRI required embryos to be removed from the egg shell (Janse and Jeurissen 1991a; Goodall, Kisiswa, Prashar, Faulkner, Tokarczuk, Singh, Jonathan T. Erichsen, et al. 2009; Zhang, T. Mesud Yelbuz, et al. 2003; Seth W. Ruffins et al. 2007; Sawamura, Takahashi, Kathryn J. McCarthy, et al. 2006) or perfusion with fixatives (Zhang, T. Mesud Yelbuz, et al. 2003; B. Hogers et al. 2001), which causes death of the embryos making repeated and dynamic observation impossible. However, in recent years, one specific approach has been investigated for immobilization of the chick embryos during scanning, which is pre-cooling. Cooling of the embryo before scanning has been introduced as a promising immobilization method (Bain et al. 2007). Bain et al. suggested to cool eggs at 4°C for one hour before scanning, which is easy to handle and appears safe (Bain et al. 2007) for the embryo. The suggested protocol, however, turned out to be incomplete since it was not adapted for the chick embryos' age and the duration of the immobilization was insufficient for high-resolution imaging especially in older embryos (Zhou et al. 2012). An age-adapted protocol was suggested by Hogers et al

(Hogers et al. 2009). They recommended exposing the embryo to room temperature prior to scanning for an age-adapted time. However, their protocol could only be applied to embryos up to d11 requiring an already very long precooling time of more than 200 minutes. Xu et al. developed an alternative approach, in which the eggs were additionally wrapped in an ice-filled foil during scanning after cooling for 1 hour (Xu et al. 2012). The suggested method enabled longer scanning times, but limited the inner diameter of the MR (Magnetic Resonance) receive coil. Larger coil diameters were required to fit the embryo and the ice, sacrificing signal to noise ratio (SNR) and thus resolution.

Anesthesia is also a further option for chicken embryo immobilization. The biggest advantage compared to pre-cooling is that anesthesia is time-saving. Cooling time as much as one hour would not be needed if anesthesia effect could be reliable. But unlike most of other in vivo models, for chicken embryo it is not possible to inject anesthetics subcutaneously, intraperitoneal, or intravascular. The most often used protocol is to drop liquid anesthetics directly onto CAM or to use gas anesthetics. As a reference, Alexander Heidrich et al (Heidrich et al. 2011) have already investigated the effectiveness and side effect of Isoflurane, UC (Urethane/ $\alpha$ -chloralose) anesthetic and Avertin application in chicken embryo model. Andreas Boss et al (Boss et al. 2008) used Ketmin for embryo immobilization. In our investigation all these fluid and gas anesthetics mentioned above were tested alone, combined, and in consideration with pre-cooling, to identify an optimal immobilization protocol.

### 1.3.3 Investigated MRI techniques

With the modified immobilization protocol, high spatial resolution of anatomical features and MR properties of in ovo grown tumor xenograft by MRI become feasible. This study shows the feasibility of applying high-fidelity serial MR imaging for in ovo MRI analysis of cancer xenograft on the chick chorioallantoic membrane.

### **1.3.3.1 High resolution of anatomical features and growth monitor of cancer xenograft on CAM**

A conventional turbo spin echo sequence was used to monitor, record, and analyze the anatomical features and growth progress of breast cancer xenograft on the CAM. These data can be used to visualize morphological information of breast cancer xenograft on the CAM and compare with the data of breast cancer xenograft in nude murine models published earlier. Tumor growth monitor is important because the data could be used as reference in the assessment for novel antineoplastic therapies (drugs, radiotherapy, chemotherapy) using CAM assay.

### **1.3.3.2 T<sub>2</sub> maps and DWI analysis of cancer cell xenograft on CAM**

The image contrast on T<sub>2</sub>-weighted images is determined mainly by tissue-specific T<sub>2</sub> relaxation times. Increased tissue water and blood volume is known to increase T<sub>2</sub> relaxation time (Oh et al. 2005). Animal models showed intermediate T<sub>2</sub> relaxation times in tumor tissue, and longest T<sub>2</sub> relaxation times in allantoic fluid (Hoehn-Berlage et al. 1992; Boss et al. 2008). Therefore, a quantitative approach measuring T<sub>2</sub> relaxation times as absolute numbers in milliseconds (quantitative MRI) is the most direct and objective way to determine the image contrast in T<sub>2</sub>-weighted images of tumor tissues xenograft on CAM in ovo.

Diffusion-weighted MR imaging (DWI) is feasible imaging method for assessing both the morphological and functional aspects of mammary cell carcinomas. DWI is a MRI technique that allows quantification of the diffusion of water molecules in tissues using the apparent diffusion coefficient (ADC). Previous studies demonstrated that tumors with high ADC values are less likely to respond to chemo-radiation (Hatakenaka et al. 2008; Chawla et al. 2013), possibly because a high ADC value may reflect the presence of micro-necrosis and, consequently, increased resistance to the delivery of cytotoxic drugs as well as oxygen during chemo-radiation.

It has been shown that quantitative T<sub>2</sub> mapping and DWI is useful to monitor initial effects of anticancer therapy, and early changes in T<sub>2</sub> relaxation times and ADC seem

to be predictive of outcome (Ellingson et al. 2012; King et al. 2010). Therefore, we aimed to evaluate T<sub>2</sub> mapping and DWI techniques in the breast cancer xenograft on CAM in ovo, which can be used as reference for future assessment of novel anticancer therapies.

### **1.3.3.3 Contrast agents assessment of breast cancer cell xenograft on CAM**

Since healthy and pathological tissues possess similar MR properties, they may show poor image contrast. To improve image contrast, MRI contrast agents (CA) may be applied. There are two major classes of MRI contrast agents: positive contrast agents increasing the signal in T<sub>1</sub>-weighted sequences, and negative contrast agents decreasing the signal in T<sub>2</sub>-weighted sequences. Depending on the type of contrast agent used, tissues with CA present as brighter or darker areas in the final MR images. The ratio between transversal and longitudinal relaxivity ( $r_2/r_1$ ) is used as a comparative criterion. Positive contrast agents produce a ratio ranging from 1.1 to 2.0, while the ratio of negative contrast agents is more than 2.0.

#### **1.3.3.3.1 Gadolinium CA bio-assessment in ovo**

Gadolinium complexes are by far the most widely used positive contrast agents in clinical practice (Bottrill, Kwok, and Long 2006). With seven unpaired electrons, Gd<sup>3+</sup> possess a large magnetic moment (7.94  $\mu_B$ ) and features slow electronic relaxation times, about 10<sup>-9</sup> s (Merbach, Helm, and Tóth 2013; Caravan et al. 1999). Because Gd<sup>3+</sup> ions are toxic for animals and also human, they are mostly linked into complexes with chelates (DTPA, DOTA, etc.) prior to in vivo application. Chelates of Gd<sup>3+</sup> are currently used in nearly half of all diagnosis MRI procedures, also for breast cancer (Leach et al. 2003).

##### **1.3.3.3.1.1 Commercial Gadolinium CA testing for protocol confirmation**

Since CAM model has never been used for MRI CA assessment with intravascular injection protocol, there is no reference for our investigation. There have been many kinds of commercial gadolinium CA widely used in clinical patients, 3 of which were used for evaluation CA enhanced imaging in the CAM model.

**1.3.3.3.1.1.1 Vasovist® (Gadofosveset)**

Vasovist is a clinically approved gadolinium-based contrast agent that reversibly binds to serum albumin, resulting in a prolonged vascular presence and a 5-fold to 10-fold increase in relaxivity ( $r_1$ ) (Goyen 2008). Vasovist is a blood-pool agent, which means it stays in blood circulation for longer time than many other kinds of CA and may have higher likelihood to enter the xenograft tumor tissues through leaky neo-vessels.

**1.3.3.3.1.1.2 Dotarem® (Gd-DOTA/Gadoterate meglumine)**

Dotarem is a macrocycle-structured gadolinium-based MRI contrast agent. It consists of the organic acid DOTA as a chelating agent, and gadolinium ( $Gd^{3+}$ ), and is used in form of the meglumine salt (Herborn et al. 2007). The drug is approved and used in a number of countries worldwide. Its paramagnetic property reduces the  $T_1$  relaxation time (and to some extent the  $T_2$  and  $T_2^*$  relaxation times) in MRI. It is used to assist imaging of blood vessels and of inflamed or diseased tissue where the permeability of blood vessels becomes higher. So it was also supposed to work for breast cancer cell xenografts.

**1.3.3.3.1.1.3 Multihance® (Gadobenate dimeglumine)**

Multihance is currently used in clinical routine mainly for MRI of the central nervous system (CNS) and also Magnetic Resonance angiography (MRA) (Pintaske et al. 2006). MultiHance also provides high relaxivity (Achenbach et al. 2010) and has demonstrated excellent diagnostic performance in MRA (Gerretsen et al. 2010) to evaluate adults with known or suspected occlusive vascular disease. MultiHance demonstrates weak and transient interactions with serum proteins that cause slowing in the molecular tumbling dynamics. Because of this interaction with serum proteins, MultiHance offers the high relaxivity which means a great ability to shorten proton relaxation times, and to increases signal intensity on  $T_1$ -weighted MR-images (Giesel et al. 2006; Rohrer et al. 2005).

### **1.3.3.3.1.2 cHSA-PEO(2000)<sub>16</sub>-Gd-DOX<sub>27</sub> bio-distribution assessment in ovo**

After gadolinium CA in ovo protocol was confirmed, this in vivo model was finally used for one of the most important purpose of this work: novel Gadolinium CA was assessed in CAM model.

Conjugation of DOTA-Gd onto drug-carriers could overcome intrinsic limitation associated with small molecule  $Gd^{3+}$  complexes, for example the broad tissue distribution and the risk of some side effects especially for kidney diseases (Bui et al. 2010). It has been demonstrated that conjugation of  $Gd^{3+}$  to slowly tumbling objects, such as nanoparticles, liposomes, polymers, etc., could significantly improve the contrast efficiency (Cheng, Thorek, and Tsourkas 2010).

Actually, there is a kind of versatile Gadolinium carrier using the abundant plasma protein serum albumin that has been considered as a promising candidate due to its attractive biochemical and pharmacological profile (Neumann et al. 2010). Among all being developed serum albumin carried agents, cHSA-PEO(2000)<sub>16</sub>-Gd-DOX<sub>27</sub> is a newly developed nanoparticle formed by self-assembly of cHSA, PEO (Polyethylene oxide), loaded with Gd-DOTA, and also Doxorubicin which is a drug used in cancer chemotherapy (Tacar, Sriamornsak, and Dass 2013). It is a novel theranostic system with the functions both for diagnosis and therapy of cancer, which was assessed in ovo in this research. This part research was in close cooperation with Dr. Yu-Zhou Wu (Wu et al. 2013).

### **1.3.3.3.2 FeraSpin™ XS (USPIO) bio-distribution assessment in ovo**

FeraSpin XS is a kind of ultra-small super-paramagnetic iron oxide (USPIO) contrast agent for pre-clinical magnetic resonance imaging. FeraSpin XS belongs to the FeraSpin Series, which are agents of high relaxivity. It enhances the contrast in  $T_2$ - and  $T_2^*$ -weighted MRI due to a shortening of the spin-spin relaxation time ( $T_2$ ). Upon intravenous injection, all agents circulate in the blood stream and are taken up by macrophages. It accumulates in the liver and spleen and is degraded within a few

days with their iron being transferred into the physiological iron stores. The macrophage uptake varies in dependence of particle size. Increased uptake by the Kupffer cells (macrophages of the liver) with increasing particle size leads to a rapid accumulation in the liver and spleen and a short blood circulation time. With decreasing particle size, the uptake by the Kupffer cells is reduced leading to a prolonged circulation time and increased uptake by other macrophages.

#### **1.4 Objective of the thesis**

In summary, it was the aim of this thesis to develop an immobilization protocol for chicken embryos to evaluate high-resolution anatomic imaging and assessment of the bio-distribution of various kinds of CA after systemic injection.



## 2 Materials and Methods

### 2.1 Materials

#### 2.1.1 Fertilized Eggs

Fertilized White Leghorn eggs LSL Rhein-Main GmbH, Dieburg, Germany

#### 2.1.2 Cells

Human breast carcinoma cell line MDA-MB-231 American Type Culture Collection, Rockville, MA

#### 2.1.3 Laboratory Equipments

11.7 Tesla small animal MRI system Bruker BioSpec 117/16, Germany

Axiophot microscope Carl Zeiss, Göttingen, Germany

Cold Light Sources, KL 1500 LCD SCHOTT, Mainz, Germany

Incubator for cells Heraeus, Hanau, Germany

Incubator for eggs HEKA Brutgeräte, Rietberg, Germany

Isoflurane Vapor 19.3 Drägerwerk AG & Co. KGaA, Lübeck, Germany

Pipette Eppendorf, Hamburg, Germany

Precision balance, Precisa 321 LX 220A Precisa Gravimetrics AG, Dietikon, Switzerland

Refrigerator LIEBHERR Comfort, Bulle, Switzerland

Shaker, Voatiex-Genie 2 Scientific Industries, New York, USA

#### 2.1.4 Analysis Software

Matlab MathWorks, Natick, WA, USA

OriginPro 9.32 OriginLab, USA

ParaVision 5.1 Bruker Biospin GmbH, Rheinstetten, Germany

Segment MEDVISO AB, Lund, Sweden

SPSS 21.0 IBM Corp, Armonk, NY, USA

### 2.1.5 Consumable Items

0.01-1ml injectors	B BRAUN, Melsungen, Germany
2,2,2-tribromoethanol	Sigma-Aldrich Chemie GmbH, Germany
30G 1/2 needles	BD Microlance™ 3, BD Drogheda, Ireland
70% ethanol solution	Universität Ulm-Klinikum Apotheke, Ulm, Germany
α-chloralose	Sigma-Aldrich Chemie GmbH, Germany
Dotarem®	Guerbet GmbH, Sulzbach, Germany
EDTA	Sigma-Aldrich, Taufkirchen, Germany
Feraspin™ XS	Miltenyi Biotec GmbH, Bergisch Gladbach, Germany
Isoflurane	DeltaSelect GmbH, Germany
Ketamin	Pfizer, Berlin, Germany
Matrigel	BD Biosciences, Heidelberg, Germany
Multihance®	Bracco Diagnostics Inc., Monroe, USA
Normal saline	Fresenius Kabi Deutschland GmbH, Bad Homburg, Germany
OpSite*	Smith & Nephew, London, England
Reaction tube	Eppendorf, Hamburg, Germany
Tape, Leukopor	BSN medical GmbH, Hamburg, Germany
Tert-amyl-alcohol	Sigma-Aldrich Chemie GmbH, Germany
Urethane	Sigma-Aldrich Chemie GmbH, Germany
Vasovist®	SCHERING AG, Berlin, Germany

## 2.2 Chicken Embryos

All in ovo experiments were in compliance with the European directive for “Protection of animals used for experimental and scientific purposes” issued by the Directorate General for Environment [Directive 2010/63/EU of the European Parliament and of the Council of 22 September 2010 on the protection of animals used for scientific purposes. Official Journal L 276, 20.10.2010 p. 33-79 (revising

Directive 86/609/EEC) ] and the respective German interpretation "Tierschutz-Versuchstierverordnung vom 1. August 2013 (BGBl. I S. 3125, 3126), die durch Artikel 6 der Verordnung vom 12. Dezember 2013 (BGBl. I S. 4145) geändert worden ist". Accordingly, in ovo experiments do not require any special additional allowance as long as the embryos are sacrificed before hatching as done in this study. Fertilized White Leghorn eggs (*Gallus domesticus*) were purchased from a hatchery and maintained at 37.8°C and a 60% relative humidity atmosphere in a tabletop incubator for the whole incubation period. After incubation of the eggs for 4 days, they were gently cleaned with a 70% ethanol solution, fenestrated, and analyzed for fertilization and normal growth. Fertilization was checked by assessment of the CAM vascularization. After fenestration, the shell access windows were neatly sealed with tape to prevent contamination and placed back into the incubator. For the residual breeding time, the viability of the embryos was monitored daily by carefully checking the CAM vasculature for blood flow and physiological embryo movement. The growth of the embryos was monitored according to Hamburger and Hamilton (Hamburger and Hamilton 1951) by candling the embryos and assessment of the shadows of internal structures in comparison with embryo growth standard, by MRI analysis of the embryo morphology, and after the end of the experiment by pathological examination.

## **2.3 Immobilization protocol optimization**

### **2.3.1 Cooling Regime Optimization**

Twenty-nine chick embryos were used to optimize the cooling protocol in ovo. Three groups were formed: ten chick embryos (Group A) were kept in the incubator as control group. Ten chick embryos (Group B) followed a static cooling regime (one hour at 4°C). Nine chick embryos (Group C) were used for optimization of the proposed age-adapted cooling regime. Group C was subdivided into 3 secondary groups (C1-C3) aiming for careful prolonging of the cooling time. Each day the minimum cooling time required for complete immobilization was assessed by

monitoring the embryo over one hour by continuous MRI scanning. The following day, in subgroup C1 the same cooling time as required the day before was used, where in the other groups the cooling time was prolonged by 10 (C2) and 20 (C3) minutes. The initial cooling time chosen was 40 min (Zhang, T. Mesud Yelbuz, et al. 2003). All eggs were examined each day to confirm the viability of the embryos. The embryos were cooled immediately prior to MRI.

### 2.3.2 Immobilization using anesthetics

The protocol of Alexander Heidrich et al was taken as reference (Heidrich et al. 2011), urethane,  $\alpha$ -chloralose, tert-amyl-alcohol, 2,2,2-tribromoethanol, Ketamin, and isoflurane were commercially purchased.

The UC anesthetic was prepared as a mixture of 450 mg/ml urethane and 45 mg/ml of  $\alpha$ -chloralose. Avertin was prepared as stock solution, that is 5.0 g of 2,2,2-tribromoethanol dissolved in 3.1 ml of tert-amyl-alcohol yielding a final concentration of 1,600 mg/ml of 2,2,2-tribromoethanol. The undiluted stock solution was used for application. Ketamin was prepared in the concentration of 1:100 mixed with normal saline. Isoflurane is commercially available as ready-to-use solution.

Eight chicken embryos at day 16 of incubation were prepared for anesthetics assessment. Two eggs used for UC group, two for Avertin group, two for Ketamin group, and the other two for isoflurane. 0.5 mL UC anesthetic, Avertin, and Ketamin were applied as liquids directly onto CAM respectively. After application, the eggs were put back into the incubator for approximately 15 min to ensure the full impact of the anesthetics. For the isoflurane, the commercial veterinary anesthesia system was used. It consists of a flowmeter and a vaporizer. The vaporizer was set to deliver an isoflurane concentration of 5% with oxygen as the carrier at a flow set between 0.5 and 12 L/min. For anesthesia induction, eggs were placed into a home-built anesthesia induction chamber (inner dimensions: 180×300×210 mm) for mice and rats connected to the isoflurane system. To reach the desired isoflurane concentration of 5% within the chamber prior to the start of anesthesia induction, it

was flooded for 5 min with an oxygen flow of 5 L/min and an isoflurane concentration of 5%. After anesthetics applied, chicken embryos were monitored over one hour by continuous MRI scanning to compare the anesthesia immobilization effects.

### **2.3.3 Anesthetics application combined with pre-cooling**

To further prolong the immobilization time after pre-cooling, isoflurane was additionally applied during scanning after sufficient pre-cooling for stronger immobilization if extremely long scanning time was needed. Because CAM is quite weak and easy to be destroyed, high isoflurane concentration (5% with pure oxygen as carrier) but at very low flow rate was applied. Five chicken embryos at day 16 of incubation were used for assessment. After sufficient pre-cooling using novel designed cooling regime, eggs were scanned continuously. In the scanning progress different flow rate of isoflurane was applied for 5 eggs: 0, 0.5, 1, 1.5, 2 l/min. The possible prolongation of the motion-artifact-free scanning times was evaluated.

### **2.3.4 Assessment Criteria**

The quality of the immobilization was assessed qualitatively by monitoring motion artifacts in the resulting images.

## **2.4 Cancer Cell Grafting**

Human breast carcinoma cell line MDA-MB-231 was cultured in L-15 growth medium supplemented with 10 % (v/v) FBS. Grown cells were harvested using 0.25% trypsin/0.53 mM ethylenediaminetetraacetic acid (EDTA) and washed at 37°C in physiological saline solution before grafting.

On d7 after incubation, breast cancer cells were grafted onto the CAM of 35 eggs in total. A silicone ring of 0.5 mm thickness with a 6 mm inner diameter was placed on the chorioallantoic membrane of each egg.  $2 \times 10^6$  cells suspended in 20  $\mu$ l of 50% Matrigel were seeded within the silicone ring (Figure 2). After cell grafting, the shell access windows were covered again and the eggs were kept in the incubator (Zuo et al. 2015).

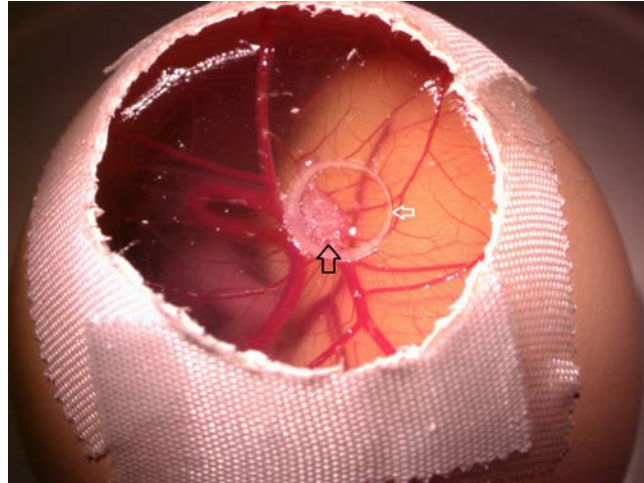


Figure 2: Breast cancer xenograft (black arrow) grew in a silicone ring (white arrow) on CAM (chorioallantoic membrane) 96 hours after grafting. Cancer cells grew in the range of silicone ring on CAM. Reproduced with permission (Zuo et al. 2015). Copyright 2015, John Wiley and Sons.

## 2.5 In Ovo MRI

### 2.5.1 MR Unit

Imaging was performed on an 11.7 Tesla small animal MRI system. The scanner comprises a superconducting magnet with a bore diameter of 160 mm. The actively shielded water-cooled gradient system operates with a maximum gradient amplitude of 750 mT/m and a slew rate of 7500 T/m/s. Data were obtained with a 60 mm quadrature volume T/R resonator (72 mm for contrast agent assessment). The eggs were placed into a custom-built polystyrene holder that was mounted on the animal support.

### 2.5.2 Tumor growth monitor

Fifteen chick embryos were used for monitoring the growth of the tumor over time. Tumor growth was monitored daily from d4 (d11) till day d9 (d16) after cancer cell grafting (incubation). High-resolution  $T_2$ -weighted images were acquired applying a multislice rapid acquisition with relaxation enhancement (RARE) sequence. Scan parameters were as follows: TR/TE = 4320/45 ms, matrix size =  $650 \times 650$ , in-plane resolution =  $77 \times 91 \mu\text{m}^2$ , slice thickness = 0.5 mm, no interslice gap, RARE factor = 8 and NSA = 4. The number of slices was adapted to the embryonic development and

ranged from 15 (d11) to 30 slices (d16). Acquisition time for a single high-resolution RARE scan resulted to from 15 to 35 minutes.

#### **2.5.2.1 Quantification of tumor volumes by MRI**

Tumor volumes were quantified by manually contouring the extent of the tumor in each slice of the MRI data sets with analysis software Segment (Partridge et al. 2005). Time-volume curves were generated by contouring the entire volume of each individual tumor. Mean volume and standard deviation were calculated for each time point. The relative growth of the tumor was assessed by normalization of the tumor volume with the initial volume, measured at d4 after tumor cell grafting. For validation of the MRI derived tumor volumes, at day 9 after grafting the region of the solid tumor component was additionally contoured for subsequent comparison with the tumor weight.

#### **2.5.2.2 Assessment of the weight of the solid tumor**

After the final MR scan at day 9 after grafting of the cancer cells, the chick embryos were sacrificed at d16 after incubation and the tumor tissues were carefully harvested from the CAM and fixed in formalin. All loose cell material attached to the solid tumor was removed before fixation. After all tumors were collected, the weight of the solid tumor tissue was measured by a precision balance.

#### **2.5.2.3 Histological Workup for anatomical comparison to T<sub>2</sub>-weighted images**

Since a heterogeneous pattern was observed in some of the MR images of the tumors, tumors were grafted on the CAM of two additional chick embryos for histological workup. MR imaging was performed as of d4 after grafting and continued daily until the inhomogeneous appearance of the tumor could be clearly appreciated in the MR images. Tissue sections were collected, paraffin embedded, and cut into 5  $\mu$ m sections. Hematoxilin (nucleus) and eosin staining (cytoplasm), proliferation Ki-67 staining (proliferation), and desmin staining (angiogenesis) were obtained, analyzed

microscopically by using an Axiophot microscope and directly compared with the respective MR images.

### 2.5.3 DWI and T<sub>2</sub> mapping

10 chick embryos were used for proving its applicability to diffusion weighted imaging and T<sub>2</sub> mapping. Diffusion weighted imaging and T<sub>2</sub> mapping was performed on d9 (d16) after cancer cell grafting (incubation). DWI was performed by a conventional diffusion prepared spin echo sequence with moderate diffusion sensitivity ( $b = 500 \text{ s/mm}^2$ ). Acquisition parameters were as: TR/TE = 5000/29 ms, matrix size = 266×250, in-plane resolution =  $200 \times 200 \mu\text{m}^2$ , slice thickness = 0.5 mm, no interslice gap, and NSA = 3. The entire embryo was covered by 30 slices with total acquisition time of TA = 60 min. T<sub>2</sub> quantification was based on data acquired by a multislice multi - spin echo technique. Acquisition parameters were as follows: TR/TE = 4000/11.1-177.6 ms (16 echoes, echo-spacing 11.1 ms), matrix size =  $512 \times 512$ , in-plane resolution =  $104 \times 98 \mu\text{m}^2$ , slice thickness = 0.5 mm, no interslice gap, NSA = 2. The area of the tumor was covered by 20 slices with an overall acquisition time of TA = 34 m8s. DWI and T<sub>2</sub> mapping images were compared to analyze the inner structure of grafted tumors.

T<sub>2</sub> values were derived from the tumor, the yolk and the albumen. For T<sub>2</sub> mapping region-of-interests were drawn manually in the respective tissues. T<sub>2</sub> values were derived by fitting a mono-exponential offset model to the resulting T<sub>2</sub> decay curve. Mean values and standard deviation were calculated.

### 2.5.4 Gadolinium contrast agent assessment in CAM model

#### 2.5.4.1 Chick embryo intravascular injection protocol

In all CA assessment experiments, chicken embryos at day 16 of incubation were used because the blood volume approaches the maximum during the incubation period (Kind 1975). After pre-cooling, the shell access windows were enlarged without hurting the CAM to facilitate the injection of the CA. The Cold Light Sources, KL 1500 LCD was used for illumination. 30G 1/2 needles and 0.01-1ml injectors were



used for injection. CA was injected into a chorioallantoic capillary vein of medium size (too big will cause worse bleeding, too tiny will increase difficulty for injection). After 5 minutes hemostasis by compression with cotton swab, around 200  $\mu$ l OpSite\* was applied to stop bleeding completely after injection. After ensuring that the bleeding was totally controlled, eggs were put back into the refrigerator before reaching suitable scanning time point.

#### **2.5.4.2 Confirmation of Gadolinium dosage for CA bio-distribution assessment with CAM model**

Vasovist was used to confirm the optimal dosage. 8 chick embryos were used for testing. After pre-cooling, 5, 10, 20, 50, 60, 70, 80, 90 $\mu$ l Vasovist were intravenously injected. Scanning was performed by a  $T_1$ -weighted three-dimensional FLASH sequence with acquisition parameters as follows: TR/TE = 6/2 ms, matrix = 400 $\times$ 439 $\times$ 96, spatial resolution = 100 $\times$ 100 $\times$ 560  $\mu$ m<sup>3</sup> and NSA = 2. Acquisition time for a single volume resulted to TA = 4min9s. After being scanned, images of 8 embryos were compared with each other to choose a dosage producing sufficient contrast.

#### **2.5.4.3 Comparison of 3 types of commercial Gadolinium CA**

Two eggs each were used to compare the SNR generated by the 3 types of CA: Vasovist, Dotarem, Multihance. The contrast agents were tested with the same gadolinium concentration. The concentrations of CA applied for each egg were as: 0.25mmol/L (Vasovist) or 0.5mmol/L (Multihance and Dotarem). The CA showing the most pronounced effect in the blood pool was chosen for systematical assessment of Gd CA bio-distribution in ovo.

#### **2.5.4.4 Identification of scanning time points**

Three chick embryos at day 16 of incubation were used for identification of the first two scanning time points after injection of commercial Gd CA of optimal dosage. Two embryos were scanned continuously from 10 minutes after injection to 110 minutes; the other 1 was scanned continuously from 60 minutes to 300 minutes. From the

time series the time points for maximum blood pool and liver contrast enhancement were identified.

#### 2.5.4.5 Systematical assessment of Gadolinium CA bio-distribution in ovo

After the dosage, CA and imaging time points for chicken embryo were identified, 10 chicken embryos at 16 day of incubation with breast cancer cell xenograft on the CAM were used for Gadolinium CA bio-distribution assessment. The imaging protocol was as: TR/TE = 6/2 ms, matrix = 400×439×96, spatial resolution = 100×100×560  $\mu\text{m}^3$  and NSA = 2. Acquisition time for a single volume resulted to TA = 4min9s. Data was acquired before and at 30 minutes, 3 hours, 5 hours, 20 hours, and 40 hours after CA injection.

SNR data of different organs (vessels, allantoic fluid, liver, and brain) of chick embryos at different time points after Gd contrast agent injection were measured and calculated. To calculate SNR, certain regions of interest (ROIs) were manually positioned by the same examiner at the same position at different time points. Special attention was paid to omit regions with artifacts. SNR was provided as mean  $\pm$  standard deviation for each investigated region. SNR was calculated according to: **SNR =  $(S_{\text{ROI}} - S_{\text{BG}}) / \delta_{\text{BG}}$**  with  $S_{\text{ROI}}$  and  $S_{\text{BG}}$  being the mean value over the ROI and background and  $\delta_{\text{BG}}$  the standard deviation of the background. An example of choosing ROIs is shown in Figure 3. As shown in Figure 3a, ROI of vessel was chosen covering most area of the umbilical vein in the liver (green). The background signal and standard deviation was derived from outside of the sample in the area with least artifact (yellow). Mean SNR and standard deviation were calculated for each time point for each egg. Time - SNR curves were generated for different embryo organs.

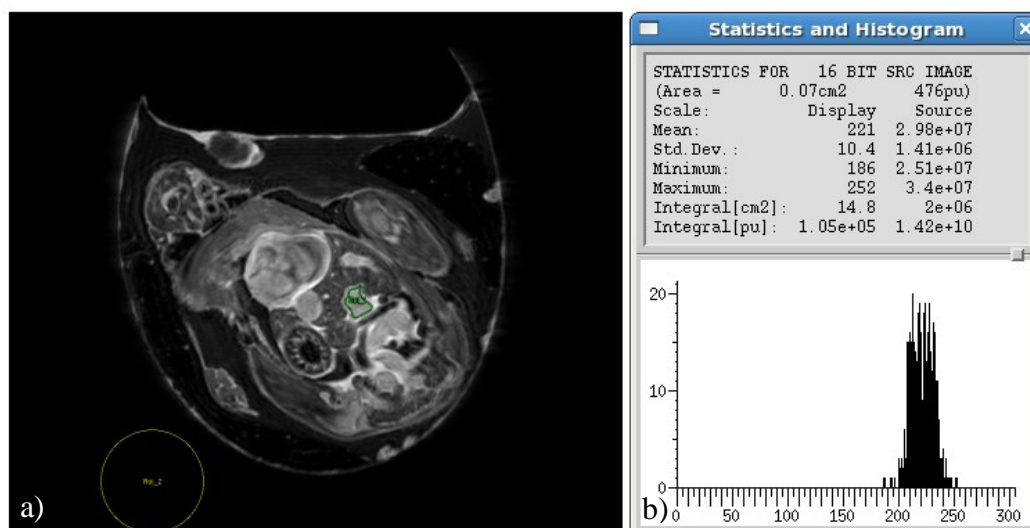


Figure 3: Example of choosing ROI (region of interest) of vessel and empty region is shown. A) ROI of vessel was chosen covering most area in the biggest vessel in liver in green color, while ROI of empty was chosen out of eggs in the area with least artifact in yellow color. B) SNR (signal to noise ratio) data could be calculated automatically.

#### 2.5.4.6 CA bio-distribution in tumor tissues on CAM analysis and histological workup

In breast cancer cell xenografts of the 10 eggs, CA bio-distribution at different time points (0, 30 minutes, 3 hours, 5 hours, 20 hours, 40 hours) was monitored, analyzed and summarized.

After scanning of 40 hours was finished, 3 solid tumors grafted on the CAM of d17 chick embryo got histological analysis. Tissue sections were collected, paraffin embedded, and cut into 5  $\mu$ m sections. Hematoxilin (nucleus) and eosin staining (cytoplasm), proliferation Ki-67 staining (proliferation), and desmin staining (angiogenesis) were obtained, analyzed microscopically by using an Axiophot microscope, and directly compared with the respective MR images at different time points to get to know better about breast cancer cell xenograft on CAM.

#### 2.5.4.7 Novel Gadolinium conjugated micelles assessment

One of the most important potential applications for the CAM model is the assessment of novel MR contrast agent particles and micelles. cHSA - PEO

(2000)<sub>16</sub>-Gd-DOX<sub>27</sub> was assessed in ovo. This project was performed in close cooperation with Dr. Yu-Zhou Wu and Ms. Wei-Na Liu.

#### **2.5.4.7.1 Preparation of cHSA-PEO (2000)<sub>16</sub>-Gd-DOX<sub>27</sub>**

cHSA-PEO (2000)<sub>16</sub>-Gd-DOX<sub>27</sub> was prepared according to the protocol of Yu-Zhou Wu, et al (Wu et al. 2013). HSA was cationized to obtain cHSA. cHSA was made completely dissolve in degassed phosphate buffer (50 mM, pH 8.0), followed by adding MeO-PEO2000-NHS dissolved in dimethylsulfoxide (DMSO) and stirring for 2 hours. After reaction, cHSA-PEO (2000)<sub>16</sub> was washed with deionized distilled water using Vivaspin 20 (MWCO 30k) centrifugal concentrator and then lyophilized to obtain cHSA-PEO (2000)<sub>16</sub>. DOTA-Gd was then conjugated onto cHSA-PEO (2000)<sub>16</sub> via coupling to amino groups on the protein surface. The synthesis of DOTA-Gd being conjugated is shown in Figure 4. Up to 85 DOTA-Gd could be incorporated into the complex. cHSA-PEO (2000)<sub>16</sub>-Gd was dissolved in degassed urea-phosphate buffer (50 mM phosphate buffer, pH 7.4, 5 M urea and 2 mM EDTA) and stirred at room temperature for 15 min. Then, DOX-EMCH was added and stirred under argon atmosphere overnight. Thereafter, the reaction mixture was purified by ultrafiltration with urea-phosphate buffer (10 mM phosphate buffer, pH 7.4, 5 M urea and 2 mM EDTA) 3 times and with water > 5 times until no red color was observed in the filtrate, then lyophilized to obtain cHSA-PEO (2000)<sub>16</sub>-Gd-DOX<sub>27</sub> as red solid. The resulting DOTA-Gd and DOX conjugated PbP (cHSA-PEO(2000)<sub>16</sub>-Gd-DOX<sub>27</sub>) self-assembled into nanosized core-shell structures in aqueous solution with the hydrophilic PEO shell outside and hydrophobic imaging and therapeutic core pointing to the inside from the protein backbone (Figure 4).

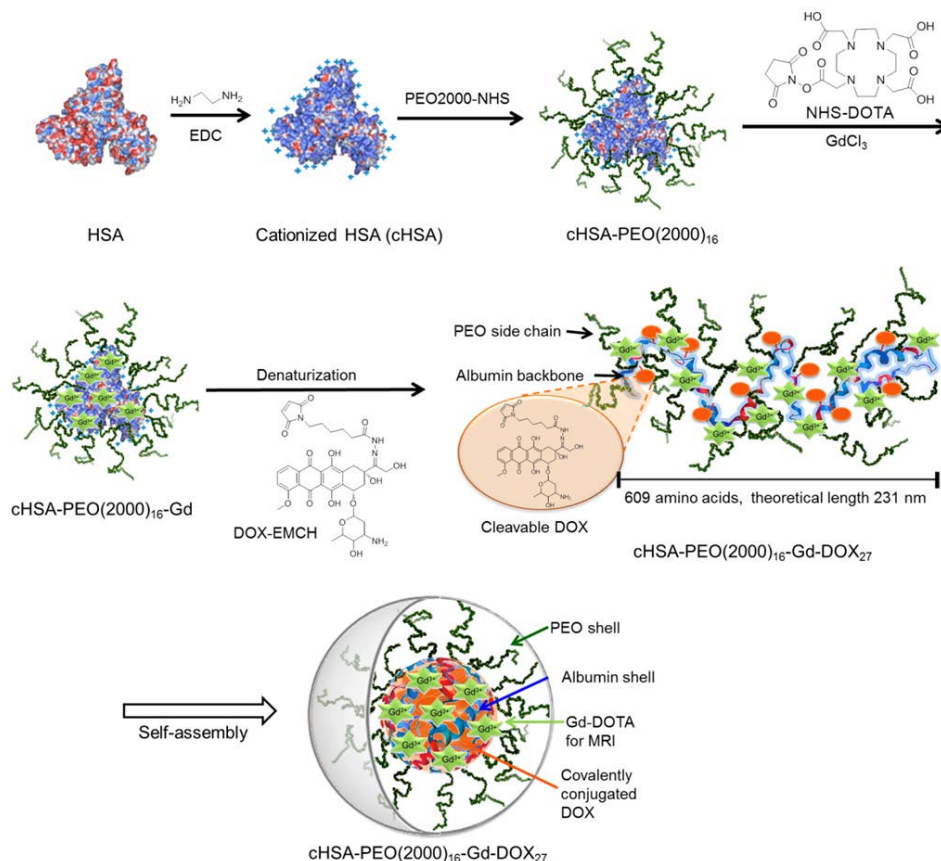


Figure 4: Preparation of Gd (Gadolinium) and DOX (Doxorubicin) loaded micelles cHSA-PEO(2000)<sub>16</sub>-Gd-DOX<sub>27</sub>. HSA: human serum albumin, DOTA: 1,4,7,10- tetraazacyclododecane-1,4,7,10- tetraacetic acid. MRI: magnetic resonance imaging. Adapted with permission (Wu 2013).

This system combined the advantages of the two-step controlled release as discussed by Yu-Zhou Wu (Wu 2013) as well as ultrasensitive MR imaging due to the high number of DOTA-Gd.

#### 2.5.4.7.2 Relaxivity measurements

The efficiency of the MR contrast agent was assessed based on its longitudinal and transverse relaxivities- $r_1$  and  $r_2$ , which reflect the ability of the contrast agent to alter  $T_1$  and  $T_2$  respectively. Relaxivity was calculated through linear least-squares fitting of  $1/\text{relaxation time (s}^{-1}\text{)}$  in different gadolinium concentrations (mM Gd). The relaxivity of DOTA-Gd loaded PbP (Protein based polypeptide copolymer) was derived. Since

Gd<sup>3+</sup> complexes are T<sub>1</sub>-type positive contrast agents, the longitudinal relaxivity  $r_1$  was calculated by plotting  $1/T_1$  as a function of Gd<sup>3+</sup> concentration.

All samples were measured at room temperature. The T<sub>1</sub>-weighted images were acquired with a conventional spin echo acquisition (TE = 11 ms) with TR values ranging from 20 to 1000 ms. Relaxivity values ( $r_1$ ) were determined from a dilution series containing Gd concentrations from 15  $\mu$ M to 200  $\mu$ M 0.9% NaCl aqueous solution. The T<sub>1</sub> values for the samples were calculated by a three parameter exponential fit applying a Levenberg-Marquardt optimization algorithm. The longitudinal relaxation rate ( $1/T_1$  in s<sup>-1</sup>) was plotted vs. the Gd concentration (mM) in PbP, and the slope was calculated according to give the value of  $r_1$  relaxivity.

#### **2.5.4.7.3 In ovo assessment of cHSA-PEO(2000)<sub>16</sub>-Gd-DOX<sub>27</sub>**

##### **2.5.4.7.3.1 Comparison of PbP produced with 2 different Gd concentration**

Two Gd concentration of cHSA-PEO (2000)<sub>16</sub>-Gd-DOX<sub>27</sub> were tested: 1mM and 3.6mM. 50  $\mu$ L and 100  $\mu$ L micelles of 1mM Gd concentration were injected into 2 eggs, while 50  $\mu$ L PbP of 3.6 mM Gd concentration were injected into the third egg. Enhancement produced by different concentrations of micelles was compared.

##### **2.5.4.7.3.2 Comparison of enhancement utility between cHSA-PEO (2000)<sub>16</sub>-Gd-DOX<sub>27</sub>, Vasovist and Multihance**

Seven eggs were used for comparison of the efficiency of cHSA-PEO (2000)<sub>16</sub>-Gd-DOX<sub>27</sub>, gadofosveset, and gadobenate dimeglumine with the same Gd concentration. 50 $\mu$ L cHSA-PEO (2000)<sub>16</sub>-Gd-DOX<sub>27</sub> with 3.6mM Gd concentration was injected into 3 eggs with cancer cell xenograft on the CAM, while 50 $\mu$ L gadofosveset solution with the same Gd concentration (0.72 $\mu$ L pure gadofosveset) and 50 $\mu$ L gadobenate dimeglumine solution with the same Gd concentration (0.36 $\mu$ L pure gadobenate dimeglumine) was injected into 2 eggs each. Images were compared both for enhanced areas and time course of the enhancement.

### 2.5.5 USPIO (Feraspin™ XS) bio-distribution assessment in ovo

Three eggs at day 16 of incubation were used for assessment of Feraspin XS bio-distribution in ovo. MRI scanning was performed 30 min, 3, 5, 10, 24 hours post-injection. A series of  $T_2$ -weighted images were acquired using  $T_2$ -weighted RARE sequence. Scan parameters were as follows: TR/TE = 3589/12 ms, matrix size = 400 × 400, in-plane resolution = 125 × 148  $\mu\text{m}^2$ , slice thickness = 0.5 mm, no interslice gap, RARE factor = 8 and NSA = 4. 30 slices were used. TA = 11 minutes.

$T_2$  quantification was based on data acquired by a multislice multi - spin echo technique. Acquisition parameters were as follows: TR/TE = 4000/11.1-177.6 ms (16 echoes, echo-spacing 11.1 ms), matrix size = 512 × 512, in-plane resolution = 104 × 98  $\mu\text{m}^2$ , slice thickness = 0.5 mm, no interslice gap, NSA = 2. The area of the tumor was covered by 20 slices with an overall acquisition time of TA = 34 m8s.

$T_2$  maps were then calculated by pixelwise mono-exponential with offset fitting to the signal intensities of  $T_2$ -weighted images acquired as a function of TE (in-house developed program with MATLAB). Relaxation times  $T_2$  were converted to their corresponding relaxivities,  $R_2=1/T_2$ .

## 2.6 Statistical Analysis

Correlation of the volume of the solid tumor and the weight of the tumor after collection was assessed applying a Spearman's rho test and the significance of differences between the volume and the weight was assessed by an unrelated Wilcoxon rank sum (Mann-Whitney-U-Test) test. P-values below 0.05 were considered significant. All statistical analyses were performed with SPSS 21.0.

### 3 Results

#### 3.1 Immobilization protocol

##### 3.1.1 Novel cooling regime

One hour cooling prior to imaging (Bain et al. 2007) did not sufficiently immobilize embryos older than 10 days of incubation and clear motion artifacts could be appreciated (Figure 5) in the resulting MRI image. With the suggested age-adapted

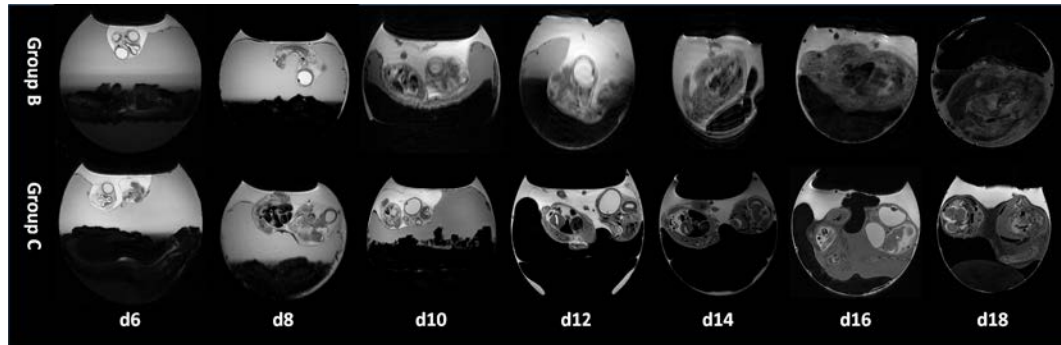


Figure 5 Representative image quality of chick embryos acquired with the different cooling protocols from d6 to d18 after incubation. Where with conventional cooling protocol (Group B) severe motion artifacts can be appreciated starting at d10, the age-adapted cooling protocol (Group C) yields artifact-free images till d18. Reproduced with permission (Zuo et al. 2015). Copyright 2015, John Wiley and Sons.

pre-cooling times as shown in Table 2, the continuous increase of cooling time enabled motion artifact free imaging for at least one hour after cooling from d6 to d18 after incubation.

The proposed cooling procedure is apparently safe for the embryos. The survival rate of the chick embryos subjected to cooling was similar to that of the control group (Table 2). In the control group (group A, 18 days of incubation, no cooling), a survival rate of 80% (8/10) was observed. Similar values of 90% (9/10) of survived embryos was observed in group B (18 days of incubation, conventional cooling for 1 h). The modified cooling protocol (group C, 18 days of incubation, age-adapted cooling) with a survival rate of 89% (8/9) did not show any obvious differences compared to the control group either.



Table 2: Minimal required cooling time necessary for immobilization of the chick embryos for at least one hour *versus* survival rate of the embryos exposed to the different cooling regimens

Days of incubation	Cooling time (minimal sufficient time, min)		
	Group A (n = 10)	Group B (n = 10)	Group C (n = 9)
6	0	60	60
7	0	60	60
8	0	60	60
9	0	60	60
10	0	60	70
11	0	60	70
12	0	60	70
13	0	60	90
14	0	60	90
15	0	60	110
16	0	60	110
17	0	60	120
18	0	60	120
<b>Survival Rate</b>	0.8 (8/10)	0.9 (9/10)	0.89 (8/9)

### 3.1.2 Immobilization with anesthetics

None of the 8 chicken embryos with application of UC, Avertin, Ketamin or isoflurane could be really immobilized to get motion-artifact-free MR images without using pre-cooling. In addition, the progress for anesthesia induction with the protocol suggested by Alexander Heidrich et al (Heidrich et al. 2011) (5% isoflurane at the flow

rate of 5L/min for 5min) wasted a big amount of isoflurane but could not truly immobilize embryos.

### 3.1.3 Isoflurane application combined with pre-cooling

After sufficient pre-cooling, additional application of high concentration (5%) at low flow rate (1 L/min is recommended) isoflurane could prolong the motion-artifact-free scanning time until 3 hours.

## 3.2 High resolution T<sub>2</sub>-weighted embryo anatomical MR analysis

The prolonged immobilization time enabled in ovo imaging with spatial resolutions as high as  $77 \times 91 \mu\text{m}^2$ . Compared to the in ovo MRI studies published previously, the higher spatial resolution resulted in clearly increased anatomical details, which can be appreciated in Figure 6. The higher image fidelity enabled detailed imaging of the tumor already at early development stage.

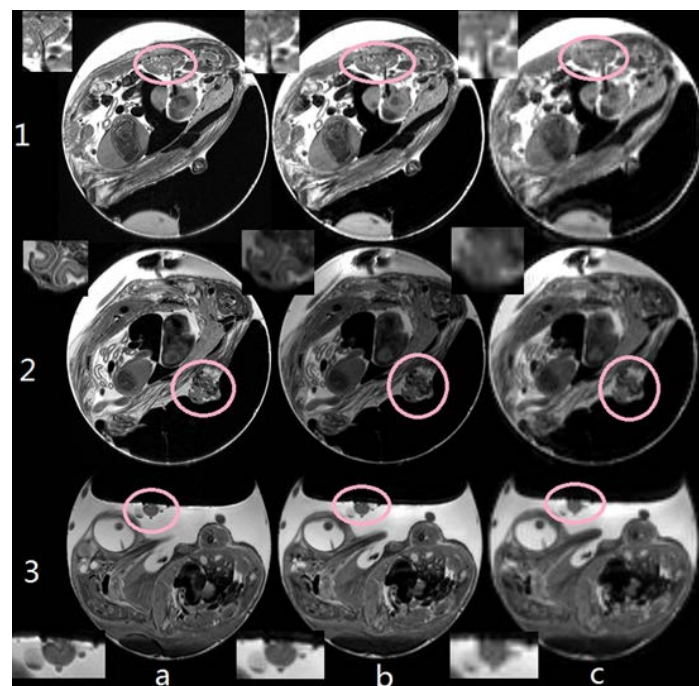


Figure 6: Comparison between different image resolutions: (a)  $77 \times 91 \mu\text{m}^2$ , (b)  $200 \times 200 \mu\text{m}^2$ , and (c)  $500 \times 500 \mu\text{m}^2$ . With increasing resolution, details of e.g. the pulmonary veins (1), the beak (2, axial orientation), and tumor tissues (3) could be clearly resolved (Circles). Reproduced with permission (Zuo et al. 2015). Copyright 2015, John Wiley and Sons.

The anatomical structure and the respective growth could be assessed from d7 to d 18 after incubation (Figure 7). At early stages of development (d7-d10), due to the

still small size of the embryo, most of the available space in the egg is still occupied by the yolk sack, allantoic fluid, amniotic fluid, and other associated fluid compartments. Clearly identifiable parts of the embryo at d7 comprised eyes, brain, and heart. At d14, the embryo had grown considerably and many other organs became visible, including the liver, gizzard, intestine, and lung tissue. The MR images allow examination of the embryo skeleton and even of the highly detailed knee joints.

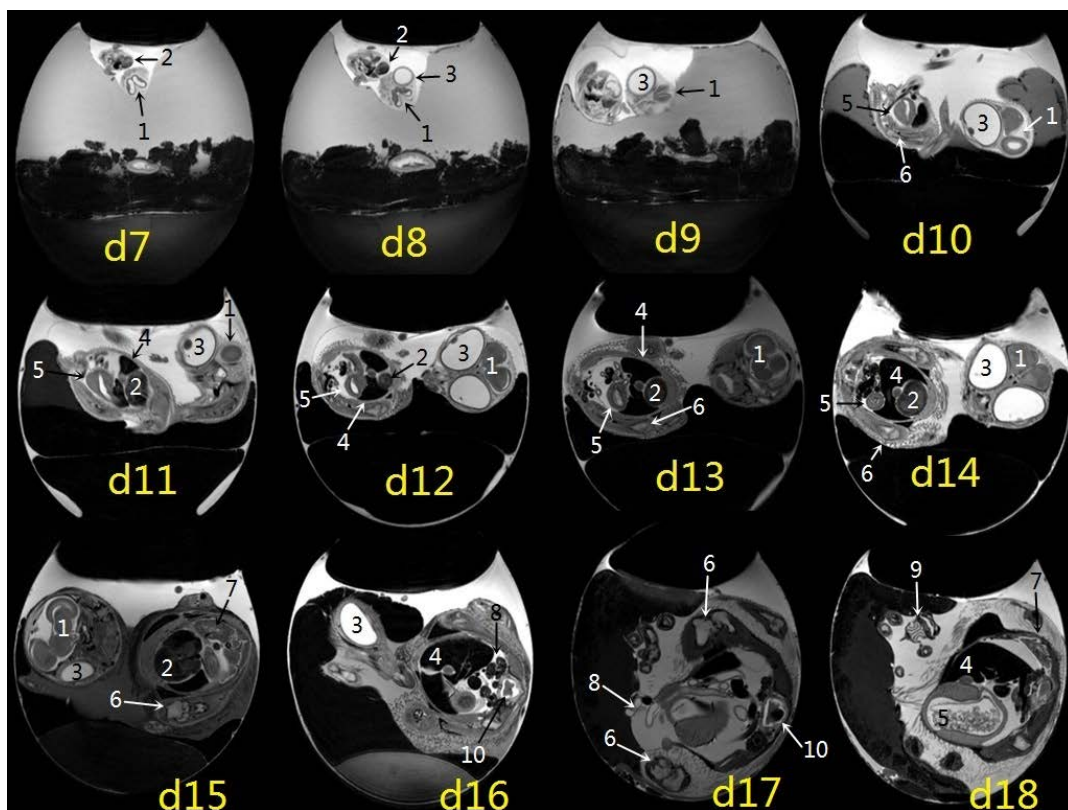


Figure 7: High anatomical details during the development and growth of different organs can be provided with high-resolution MRI (magnetic resonance imaging) between 7-18-days (d7-d18) after incubation. 1, brain; 2, heart; 3, eyes; 4, liver; 5, gizzard; 6, limb bone and knee joint; 7, lung; 8, intestines; 9, beak; 10, spine. Reproduced with permission (Zuo et al. 2015). Copyright 2015, John Wiley and Sons.

### 3.3 Tumor growth monitoring

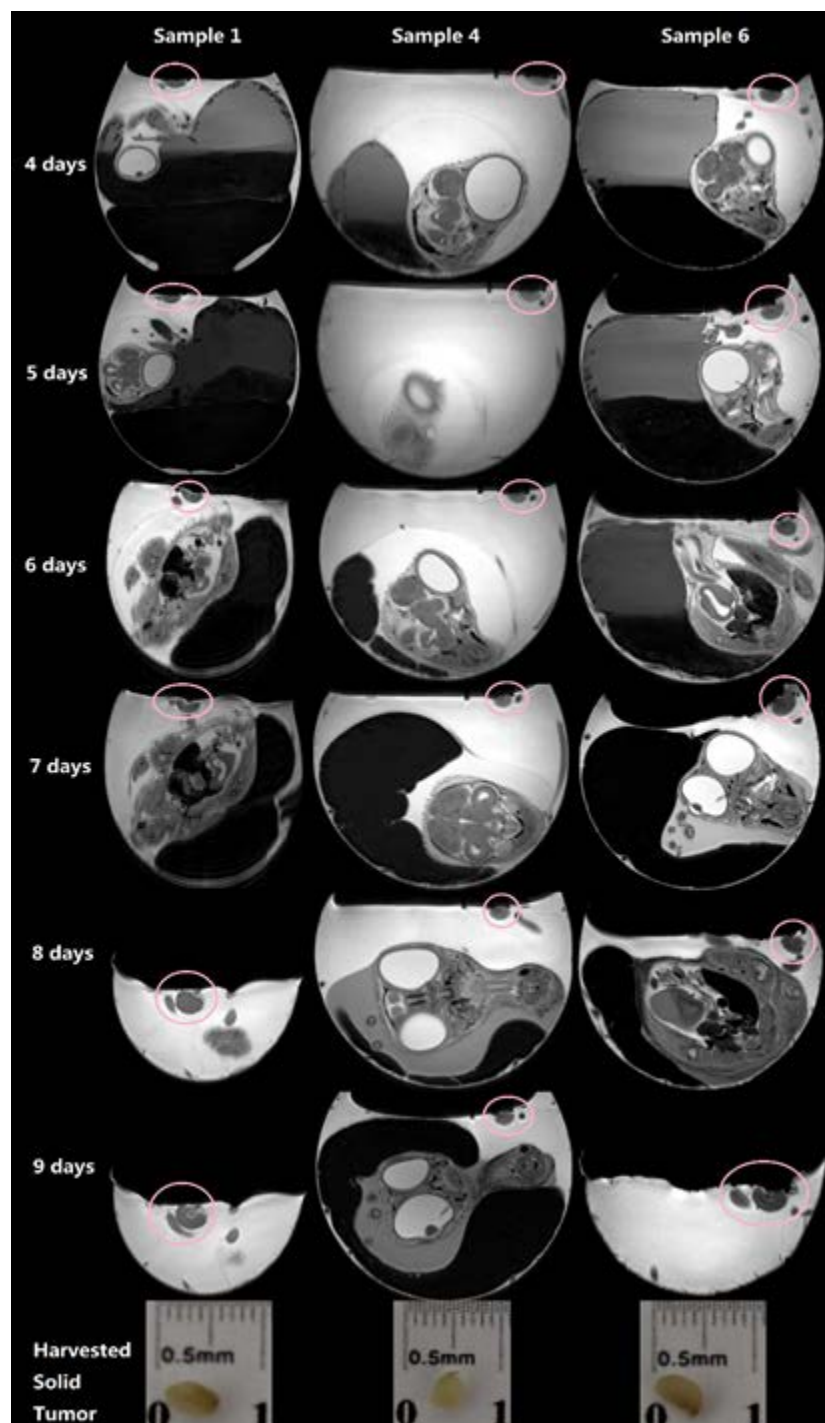


Figure 8: Longitudinal high-resolution MRI (magnetic resonance imaging) images of breast cancer xenograft (circles) grown in ovo. Breast cancer cells were grafted onto the CAM (chorioallantoic membrane) at day 7 after incubation. MRI was performed from d4 till day 9 after grafting. Reproduced with permission (Zuo et al. 2015). Copyright 2015, John Wiley and Sons.

From the 15 embryos investigated for tumor growth monitoring, two died by day 4 after grafting and four had to be excluded from further analysis, since no tumor developed. Application of the suggested MR imaging protocol for quantification of the tumor growth was successful (Figure 8). Decent image quality could be achieved in all investigated chick embryos starting from day 4 after cell grafting. The growth of each individual tumor could be quantified by applying serial MR imaging over 6 days.

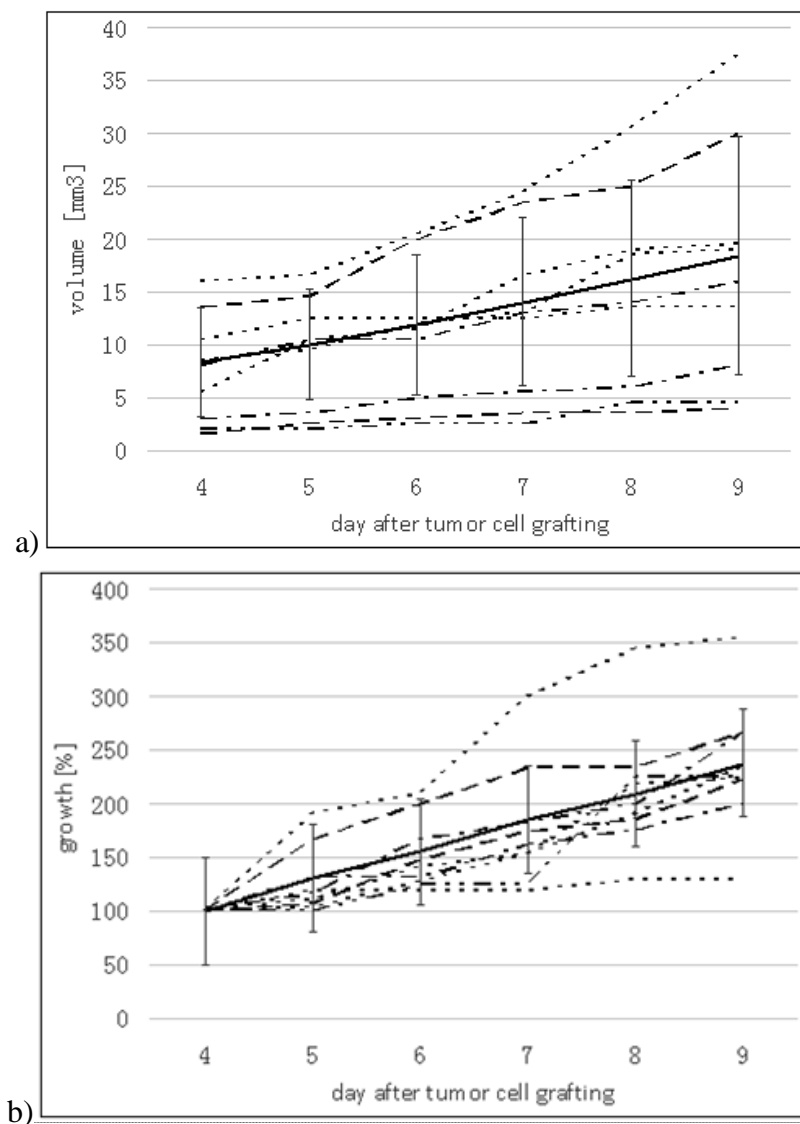


Figure 9: Volumes (a) and relative growth (b) of the breast cancer xenograft in a CAM (chorioallantoic membrane) model as analyzed by MRI (magnetic resonance imaging). Breast cancer cells were grafted onto CAM of embryos at 7-days of incubation. MRI was performed on the days 4 till 9 after transplantation. Bold line represents the mean data  $\pm$  standard deviation. Reproduced with permission (Zuo et al. 2015). Copyright 2015, John Wiley and Sons.

Even though the initial number of seeded cells was equal, the volume (Figure 9a) and growth of the tumor xenografts (Figure 9b) differed markedly between the nine investigated samples. Final overall tumor volumes resulted between 4 mm<sup>3</sup> and 37.5 mm<sup>3</sup> with a solid tumor component between 0.77 mm<sup>3</sup> and 18.77 mm<sup>3</sup> as analyzed by the volumetric quantification of the MR images.

The structure of the tumors could nicely be visualized by MRI as exemplarily shown in Figure 10 (please refer to Figure 11 for an overview of all tumors at d9 after grafting).

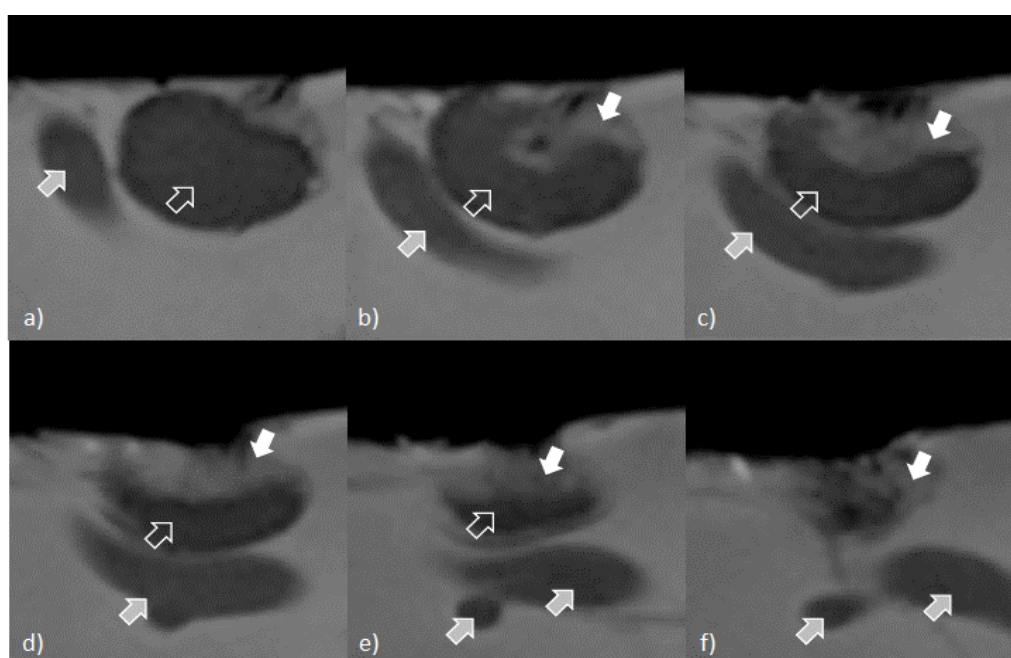


Figure 10: Subsequent sections by MRI (magnetic resonance imaging) through the grafted tumor at day 9 after tumor grafting. The solid part of the tumor (open arrow) can be clearly distinguished from unorganized cell material (white arrow) and large blood vessels (gray arrow). Reproduced with permission (Zuo et al. 2015). Copyright 2015, John Wiley and Sons.

The location of the solid tumor, uncoordinated tumor cells and blood vessels could be identified.

The MRI analysis further demonstrated that the tumor growth on the CAM had no obvious effect on the development of the major organs of the chick embryos. Similarly, we did not observe any undesired morphological alterations due to

frequent temporal cooling of the embryos. These observations were further confirmed at the end of the experiment by visual examination of the embryos.

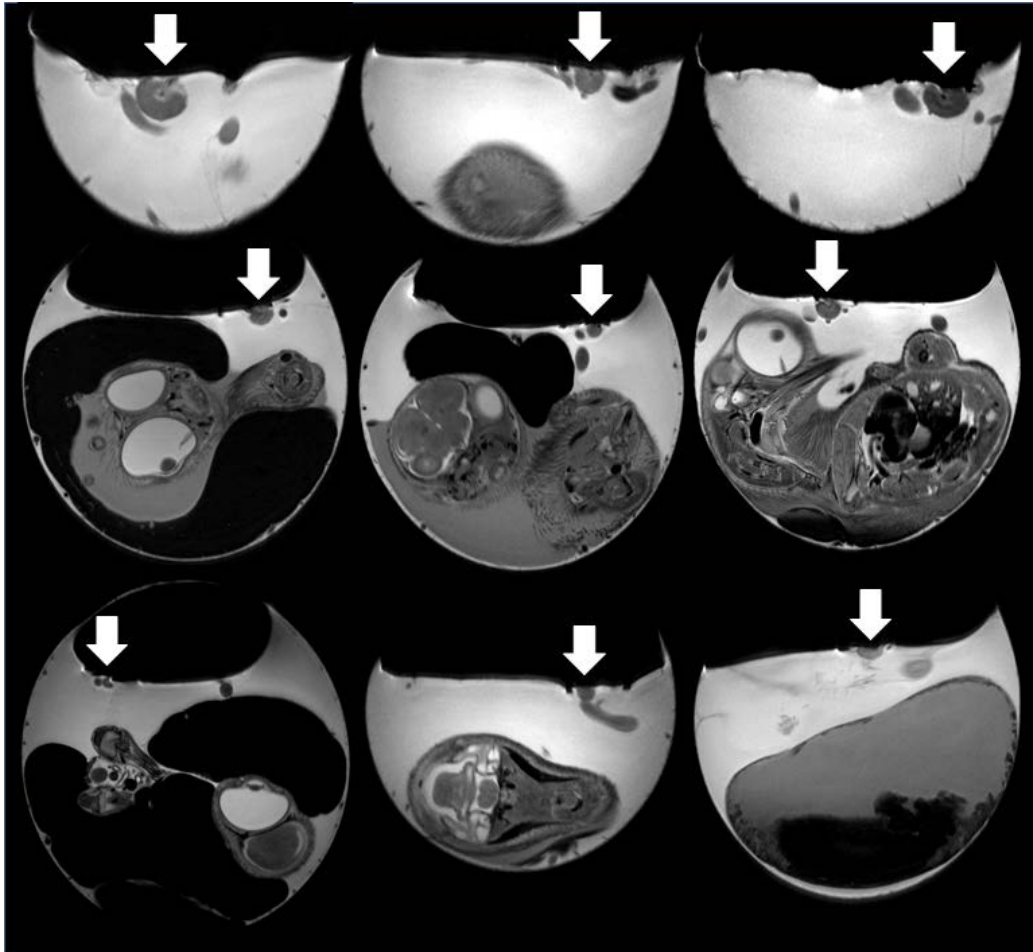


Figure 11: At day 9 after grafting (day 16 after incubation), tumors (arrows) show different volumes, structures and intensities, but are clearly visible in the T<sub>2</sub>-weighted Magnetic Resonance images. Reproduced with permission (Zuo et al. 2015). Copyright 2015, John Wiley and Sons.

At the end, i.e. at d16 after incubation (d9 after cell grafting), tumors were surgically removed and weight. Weight measurements as well as the MRI-derived volumes are shown in Table 3. Regression analysis revealed an excellent linear correlation between the two measurements ( $R^2 = 0.9$ ,  $p < 0.01$ ). The mean weight/volume ratio resulted as  $0.78 \text{ mg/mm}^3$  below the expected value of approximately  $1 \text{ mg/mm}^3$ . This difference was statistically not significant (Mann-Whitney-U-test,  $p > 0.65$ ).

Table 3: Volumes versus weight of breast cancer xenograft grown on CAM (chorioallantoic membrane) for 9 days. MRI: magnetic resonance imaging

Sample	Estimated tumor volume (MRI)	Tumor weight
No.	(mm <sup>3</sup> )	(mg)
1	18.77	13.7
2	7.76	3.7
3	6.70	3.3
4	5.99	4.7
5	1.95	2.2
6	11.19	8.6
7	8.76	5.2
8	0.77	2.6
9	1.78	2.0

### 3.4 Histological workup of breast cancer cell xenograft

The histological analysis reveals the shape and structure of the tumor as seen with MRI (Figure 12). With MRI as well as with histological analysis two different tumor components (open / closed arrow) and a large vessel can be clearly appreciated. Immunohistochemical analysis of the tumor section in contact with the CAM revealed increased cell density (Figure 12b), proliferation (Figure 12c), and angiogenesis (Figure 12d). The tumor core is necrotic, contains lesser tumor cells, exhibits lower proliferation, and almost no angiogenic blood vessels when compared to the surrounding tumor tissue. Analysis of the T2w MR images indicates its potential to delineate different components of the tumor by assessing the different



gray values of  $6855 \pm 650$  (area I in Figure 12a),  $9850 \pm 615$  (area II in Figure 12a), and  $11530 \pm 872$  in the large blood vessels beneath the tumor (area III in Figure 12a).

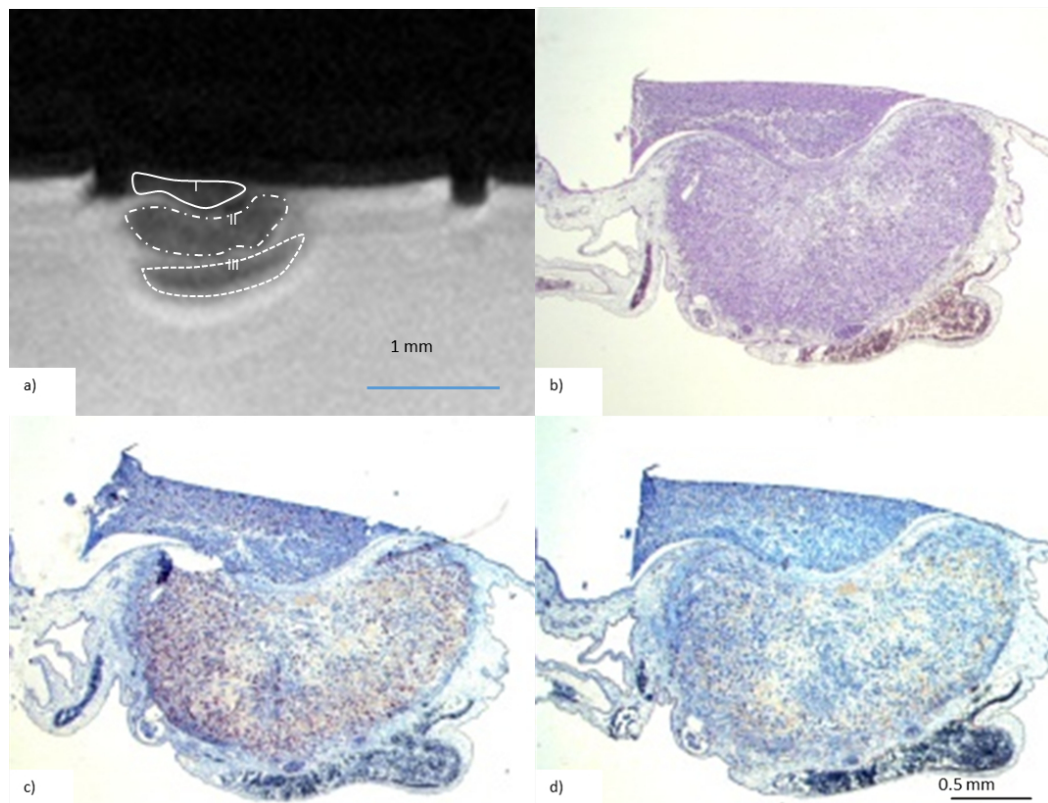


Figure 12: Correlation of immunohistological analysis (b-d) of breast cancer xenograft on CAM (chorioallantoic membrane) and MRI (magnetic resonance imaging) (a). Those areas of the tumor directly in contact with the CAM (area I in a) show higher nuclei density (b, hematoxylin and eosin staining), stronger proliferation (c, Ki-67 staining), and stronger angiogenesis (d, desmin staining) as the deeper located solid tumor (area II in a). In the respective MRI sections different gray values of  $6855 \pm 650$  (area I in a),  $9850 \pm 615$  (area II in a), and  $11530 \pm 872$  in the large blood vessels beneath the tumor (area III in a). Reproduced with permission (Zuo et al. 2015). Copyright 2015, John Wiley and Sons.

### 3.5 $T_2$ maps and DWI analysis of tumor on CAM

MR imaging could be successfully completed in all chick embryos. In all cases no motion artifacts limiting the evaluation of the images were observed even for scan times of up to 90 minutes (DWI and  $T_2$  mapping in a single session).  $T_2$  maps (Figure 13a) and DWI (Figure 13b), showed excellent image fidelity (please refer also to Figure 14).

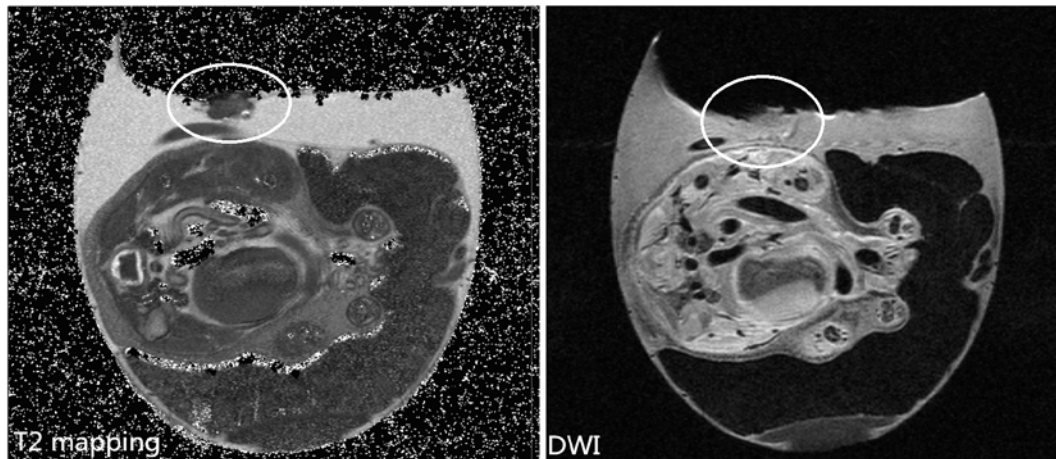


Figure 13: Example of  $T_2$  (a) and DWI(diffusion weighted imaging) mapping (b). Circles: tumors

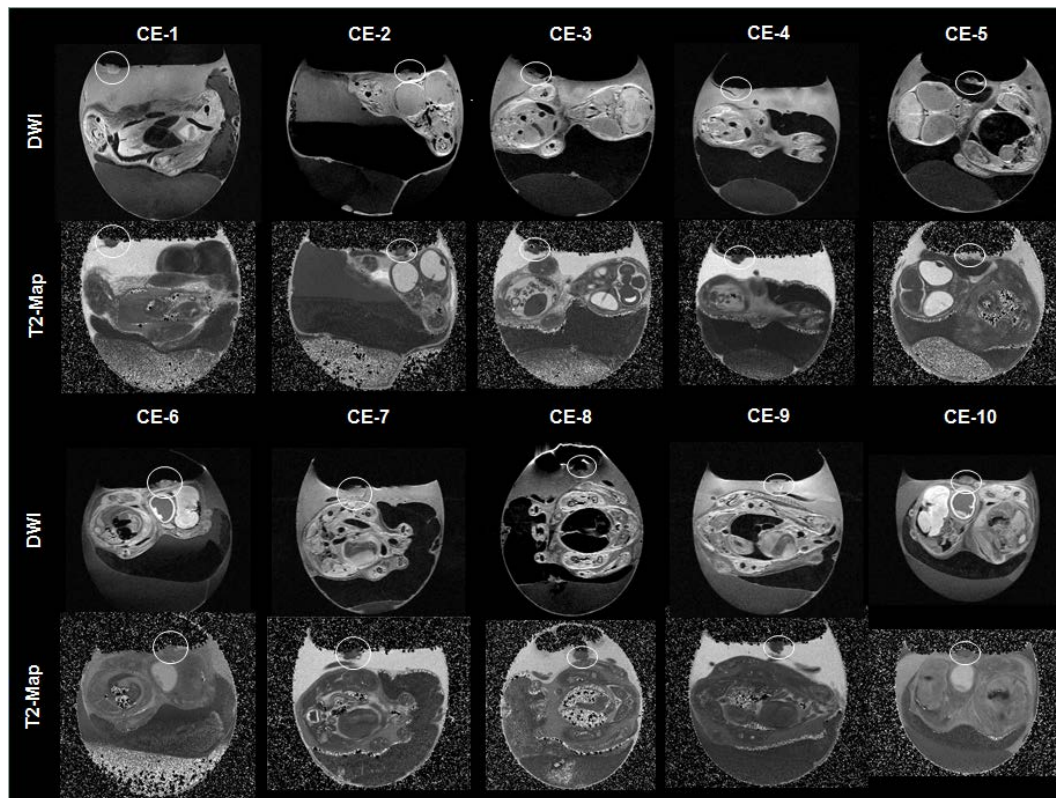


Figure 14: Diffusion weighted (DWI) images and  $T_2$  maps obtained at day 9 after tumor grafting (d16 after incubation). CE: chicken embryo. Reproduced with permission (Zuo et al. 2015). Copyright 2015, John Wiley and Sons.

In DWI as well as in the  $T_2$  maps some heterogeneity of the tumor was observed.  $T_2$  quantification revealed good reproducibility of the  $T_2$  values (tumor =  $48 \pm 2.8$  ms, albumen =  $18 \pm 2.7$  ms, yolk =  $19.6 \pm 2.7$  ms).

### 3.6 MR contrast agent assessment with CAM model

#### 3.6.1 Gadolinium CA assessment

##### 3.6.1.1 Vasovist dosage confirmation

5, 10, 20, 50, 60, 70, 80, and 90 $\mu$ l Vasovist were respectively intravascular injected into 8 chicken embryos. Images of post-injection embryos with enhanced liver vessels are shown in Figure 15. With the application of different dosages of Vasovist, blood pool of chicken embryos was enhanced in varying degrees.

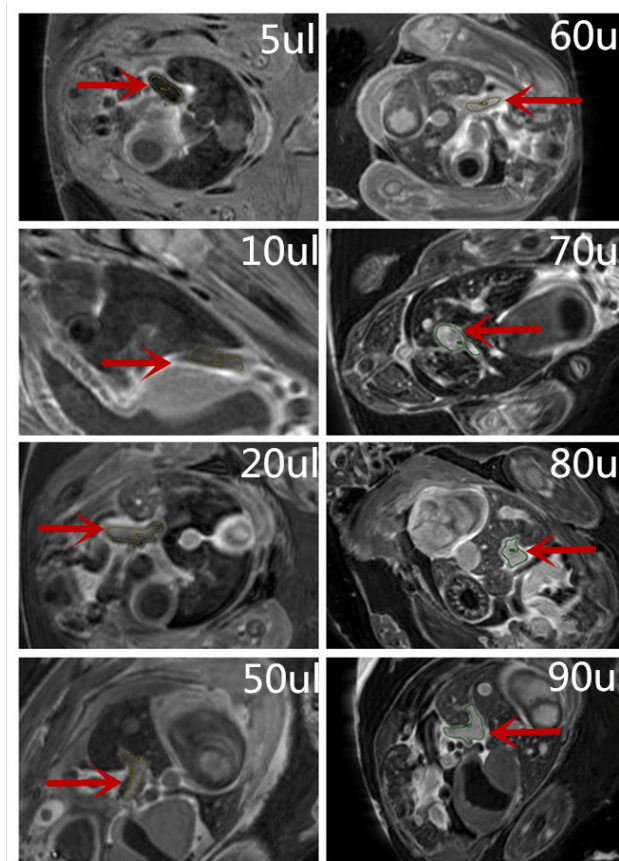


Figure 15: Images of post-injection embryos with different dosages of Vasovist, blood pool were enhanced in varying degrees. Main vessels (red arrow) in liver were chosen to calculate and compare SNR (signal to noise ratio)

Umbilical veins (red arrow in Figure 15) in liver were chosen to calculate SNR. Increasing rate of SNR of 8 samples is shown in Figure 16.

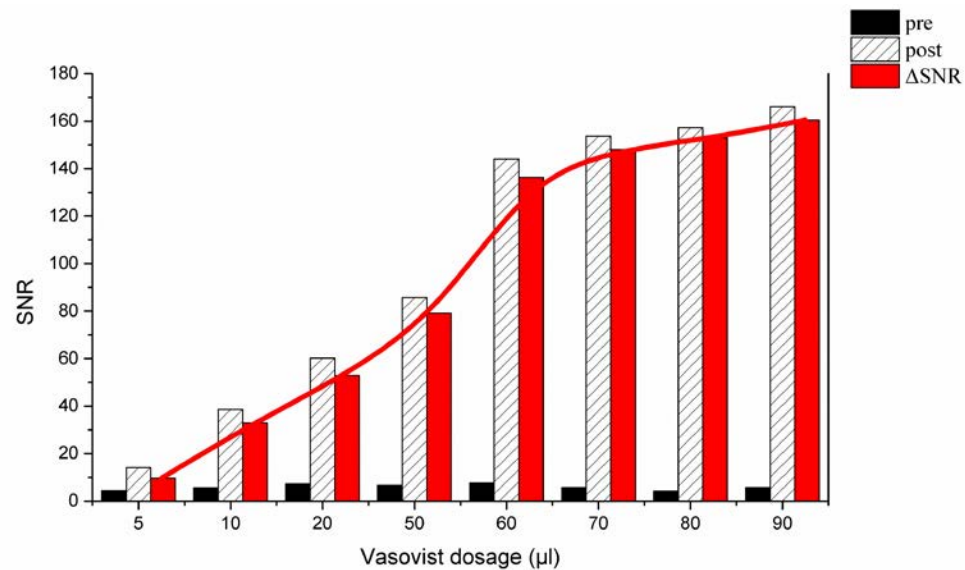


Figure 16: SNR (signal to noise ratio) of the umbilical veins post-injection of Vasovist from 5-90µl (n=8). SNR increased with increasing dosage. But the rate of increasing flattens among 70-90µl.

SNR increased with increasing dosage. But the rate of increasing flattens among 70-90µl. From this result, a dose of 80µl was chosen for subsequent experiments.

### 3.6.1.2 Comparison of 3 types of clinical authorized commercial Gadolinium CA

SNR of the blood pool of 2 CA (Vasovist, Multihance) was compared. Images are shown in Figure 17. With the same Gd concentration, Vasovist produced better contrast.

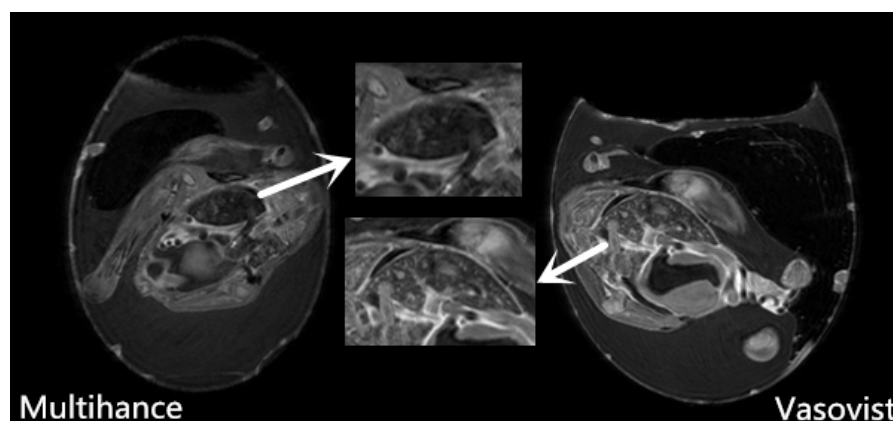


Figure 17: Comparison of images of 30 minutes after injection of Multihance and Vasovist. Enhancement in liver (arrows) produced by Vasovist was better.



At the same time, Dotarem was found to enhance some organs in the digestive system, for example the gizzard and cloaca of 2 tested embryos, which was not expected and may cause the risk of side effects and decreased survival rate after injection. Images of different organs at different time points after the application of Dotarem are shown in Figure 18.

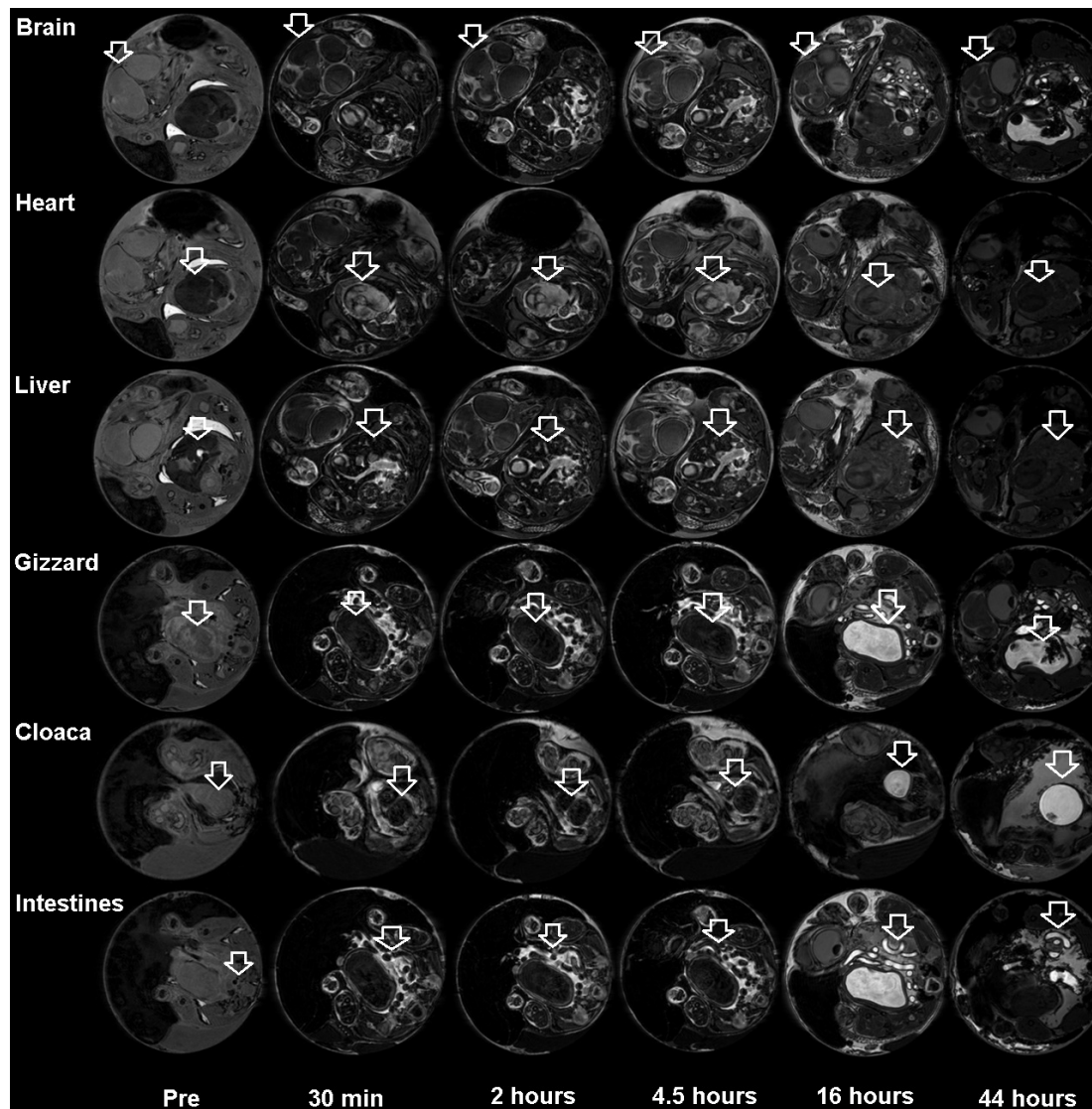


Figure 18: Images of different organs (arrows) at different time points with the application of Dotarem. Gizzard and cloaca were enhanced unexpectedly. min: minutes.

For better image quality and higher embryo survival rate, Vasovist was selected as recommended CA for subsequent chicken embryos injection.

### 3.6.1.3 Identification of scanning time points post-injection suitable for CAM model

For detailed assessment of the Vasovist bio-distribution in the CAM model, the time points for optimal enhancement need to be identified. The SNR-time curves of enhancement in blood circulation and liver parenchyma are shown in Figure 19.

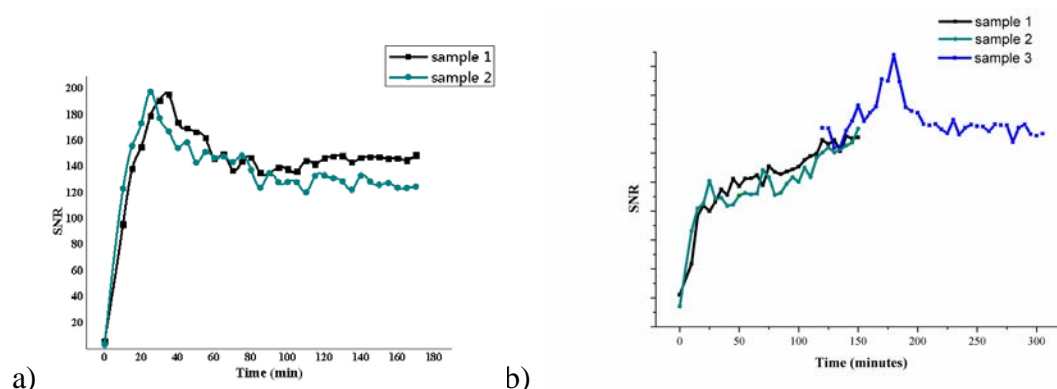


Figure 19: The SNR (signal to noise ratio) -time curves of enhancement in blood and liver. a) shows SNR changes of the blood pool from injection to 3 hours of 2 samples; b) shows SNR changes of liver parenchyma from 120 to 305 minutes post-injection.

For 2 samples used to calculate SNR of blood pool from injection to 3 hours, similar SNR peaks were found around 30 minutes after CA injection. So 30 minutes post-injection was confirmed as the peak time point for blood pool in chicken embryo model, as 3 hours was confirmed as peak time for liver parenchyma.

### 3.6.1.4 Systematical assessment of Vasovist bio-distribution in ovo

After all protocol parameters were finally confirmed, 10 embryos were used to systematically assess the Vasovist bio-distribution in the chicken embryo system. The representative sample of CA bio-distribution in different organs at different time points is shown in Figure 20.

The bio-distribution of the CA can clearly be visualized with high spatial fidelity in the FLASH images of the chick embryos. From the image it can be seen that blood pool is enhanced first, then the liver parenchyma, and at last just the allantoic fluid was enhanced.

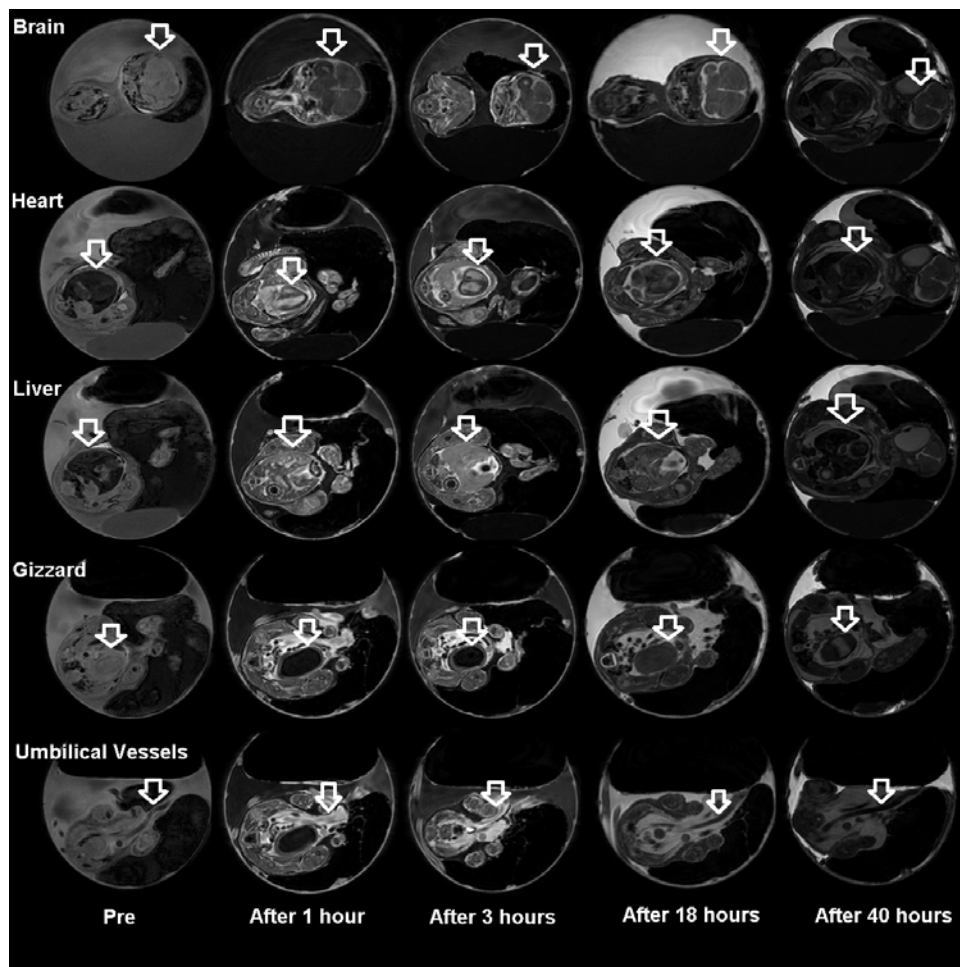


Figure 20: The representative sample of CA (contrast agent) bio-distribution in different organs (arrows) at different time points.

Change of mean SNR  $\pm$  stddev in different organs (vessels - red line, allantoic fluid - black line, liver - blue line, and brain - green line) of chick embryo at different time points after Vasovist injection is shown in Figure 21.

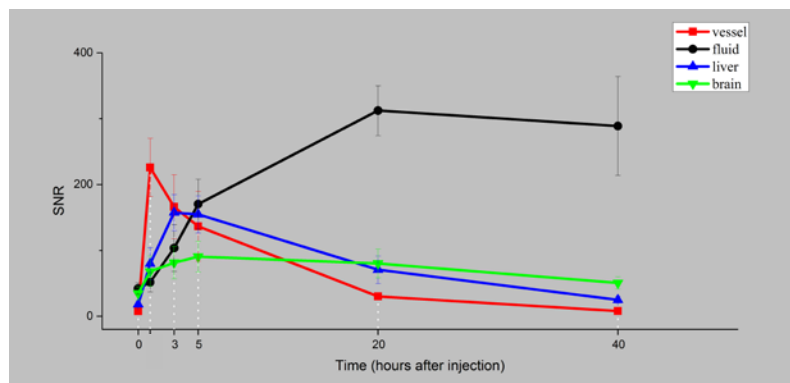


Figure 21: Change of SNR (signal to noise ratio)  $\pm$  standard deviation (stddev) in different organs of chick embryo at different time points after Vasovist injection (n=10).

### 3.6.1.5 Analysis of Vasovist bio-distribution in cancer cell xenograft on CAM

Respective images and immune-histological analysis are provided in Figure 22. A clear enhancement of the tumor can be appreciated.

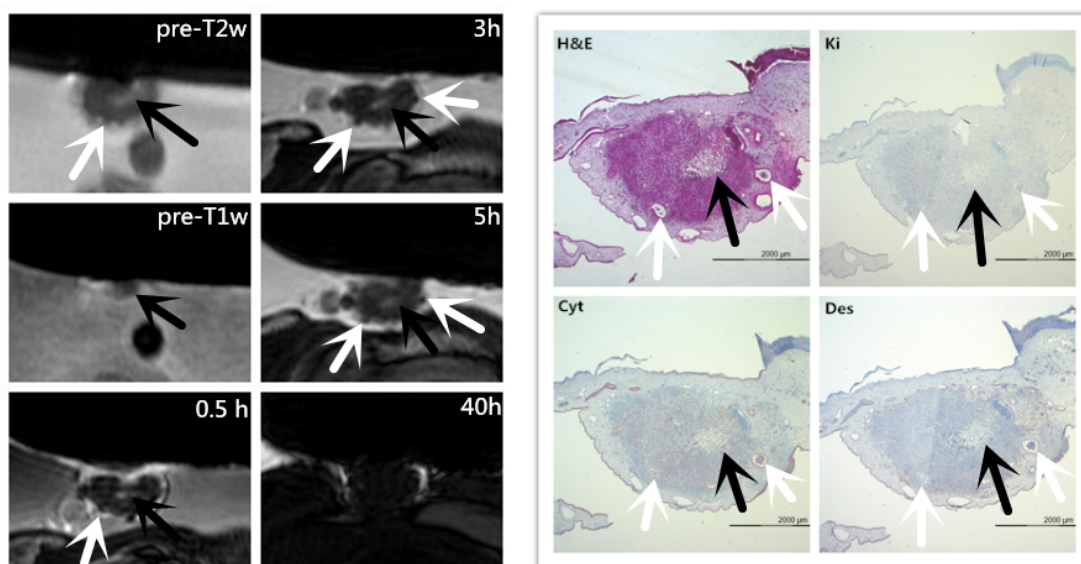


Figure 22: Correlation of immunohistological analysis, pre-CA(contrast agents) T<sub>2</sub>w anatomical image and post-CA T<sub>1</sub>w images of the tumor. h; hours. White arrow: vessel; black arrow: loose

The distribution of the systemically administered contrast agent could be clearly visualized. In direct comparison with the pre-administration situation 30 minutes after systemic injection of the blood-pool contrast agent, the uptake in the tumor could be nicely visualized, and the enhancement gradually faded out with increasing time. A clear enhancement of the border and central area of the solid tumor can be appreciated. The enhanced structures correlate well with the necrotic core and CAM as identified in the immune-histological and T<sub>2</sub> weighted images.

Images of other samples at 30 minutes post-injection are shown in Figure 23. All solid tumors show similar CA enhancement properties.



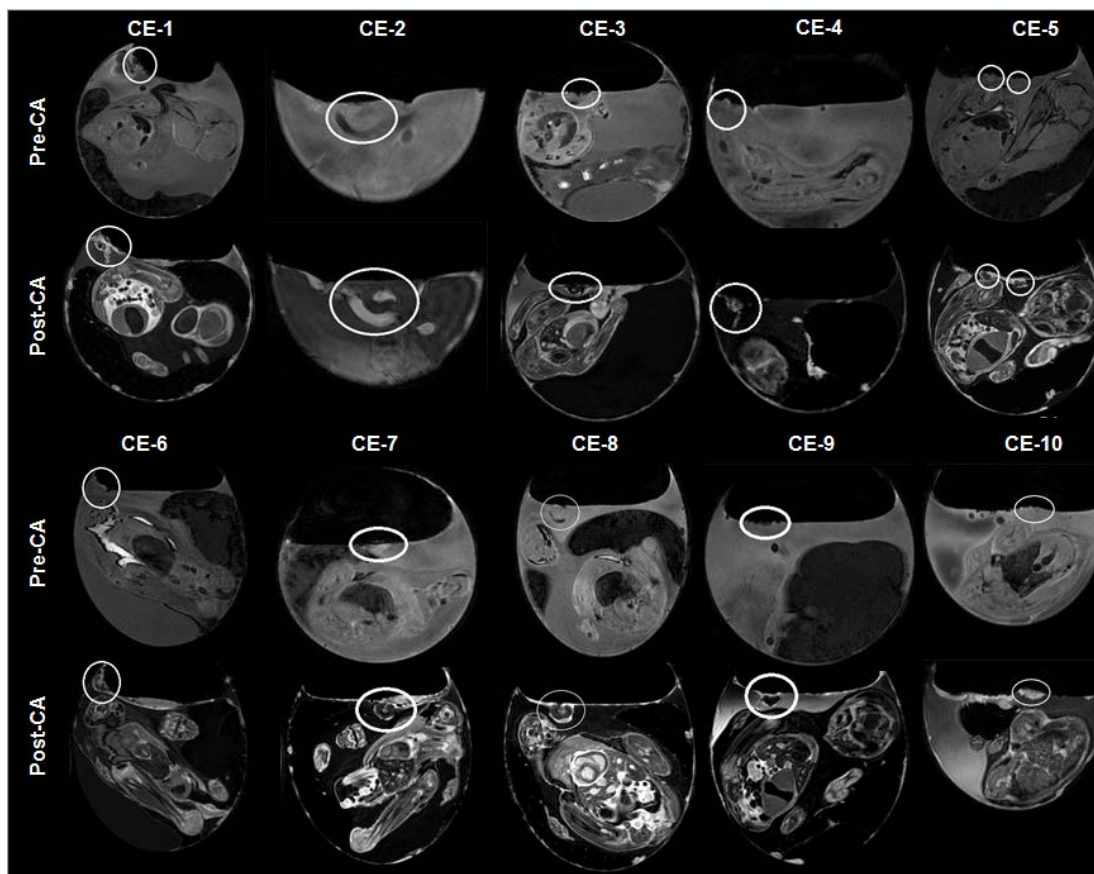


Figure 23: Images obtained pre (Pre-CA (contrast agent)) and post (Post-CA) intravenous injection of gadofosveset trisodium at day 9 after tumor grafting (day 16 after incubation). Circles: tumors. Reproduced with permission (Zuo et al. 2015). Copyright 2015, John Wiley and Sons.

### 3.6.1.6 Novel Gadolinium conjugated micelles assessment in ovo

#### 3.6.1.6.1 Relaxivity measurements

As shown in Figure 24, the linear correlation between  $1/T_1$  and  $Gd^{3+}$  concentration was observed and the value of  $r_1$  relaxivity/gadolinium was extracted from the slope of the line as  $5.93 \text{ mM}^{-1}\text{s}^{-1}$ . Compared to the  $r_1$  relaxivity of clinically used  $Gd^{3+}$  contrast agents of Gd-DOTA ( $4.3 \text{ mM}^{-1}\text{s}^{-1}$ ) and Gd-DTPA ( $4.5 \text{ mM}^{-1}\text{s}^{-1}$ ), the polymeric  $Gd^{3+}$  micelles showed increased relaxivity and hence MR efficiency. Compared to other gadolinium-based macromolecular contrast agents reported previously, the paramagnetic properties were at a comparable level.

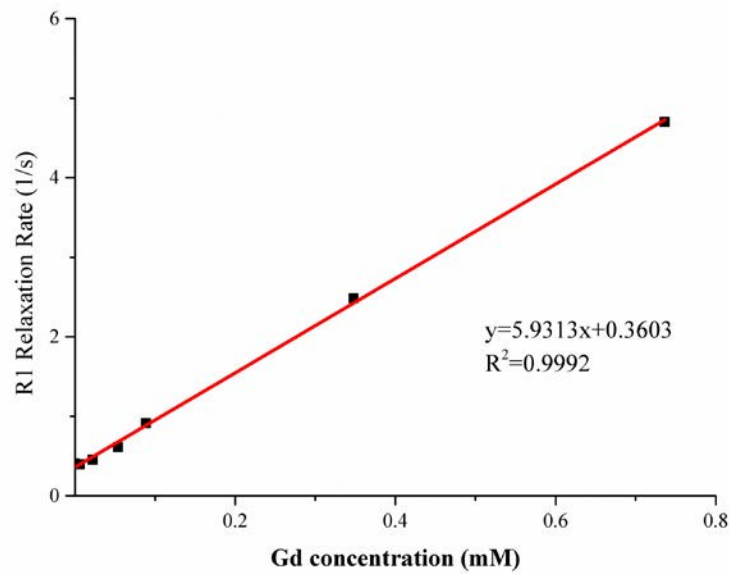


Figure 24: Relaxivity measurement of cHSA-PEG(2000)16-Gd. Gd: gadolinium.

### 3.6.1.6.2 Comparison of 2 different Gd concentration

Two different concentrations of micelles were investigated yielding molecular concentration of Gd as 1mM and 3.6mM. Micelles were injected into 2 embryos. Samples were scanned pre, 30 minutes, 2h, 6h, and 12h after injection. Images are compared in Figure 25.

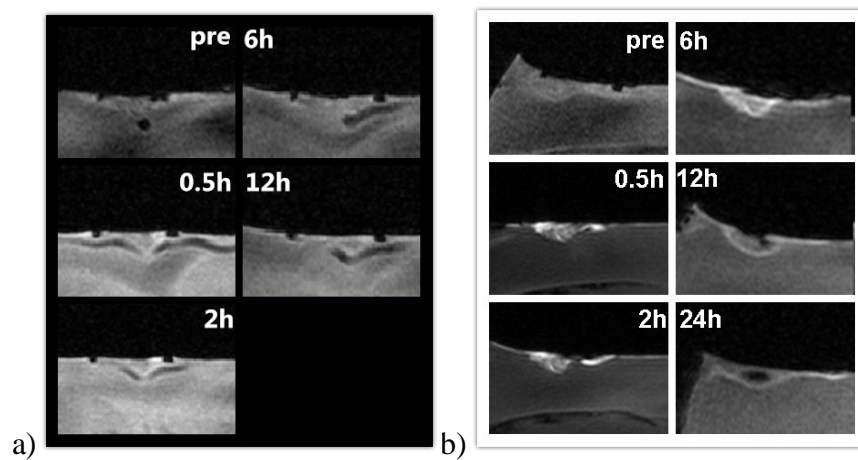


Figure 25: Comparison of enhancement effects of different Gd (gadolinium) concentration. a) shows 1mM CA (contrast agent) with which the embryo died at 24h (hours) post-injection. B) shows 3.6 mM CA long-dual enhancement effect from 0.5h until 12h.

Figure 25a shows the result of 1mM particles. After injection almost no signal enhancement can be observed in the solid tumor area. After application of PbP with 3.6 mM Gd concentration, already 0.5 h post-injection a clear enhancement of the tumor area was observed. The enhancement persisted till 12 hours after injection. The results clearly indicate the use of higher CA load of 3.6 mM cHSA-PEO(2000)<sub>16</sub>-Gd-DOX<sub>27</sub> for further experiment.

### 3.6.1.6.3 Comparison between cHSA-PEO(2000)<sub>16</sub>-Gd-DOX<sub>27</sub> and Multihance

Representative images showing the comparison of the bio-distribution of PbP, Vasovist and Multihance are provided in Figure 26.

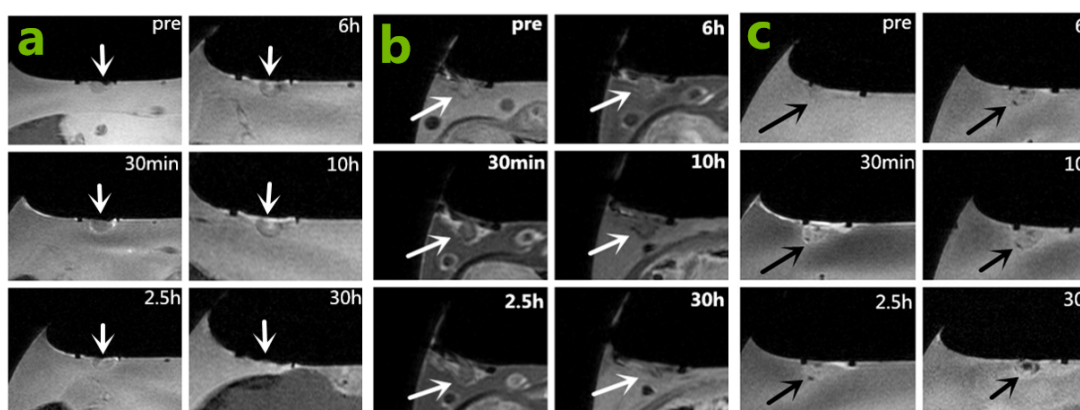


Figure 26: Comparison between cHSA-PEO(2000)<sub>16</sub>-Gd-DOX<sub>27</sub> (a), gadofosveset(b) and gadobenate dimeglumine (c). Arrows: tumors.

All 3 eggs injected with PbP showed enhancement of the tumor area. The enhancement persisted for at least 10 hours post-injection. Representative images are shown in Figure 26a. After injection of gadofosveset, only 1 tumor showed enhancement from 30 minutes to 6 hours after injection (Figure 26b). After gadobenate dimeglumine injection only a slight enhancement was observed in one tumor 30 minutes after injection (Figure 26c).

### 3.6.2 USPIO (Feraspin™ XS) bio-distribution assessment in ovo

T<sub>2</sub> map images are shown in Figure 27. The first image shows the T<sub>2</sub> map pre USPIO injection while other 5 images show different time points post-injection. There is no obvious change of T<sub>2</sub> values in the tumor area before and after CA injection, while in liver T<sub>2</sub> decreased after injection and recovered gradually.

R<sub>2</sub> map images were shown in the right column of Figure 28. After USPIO intravascular injection, the R<sub>2</sub> values of an area in the border part of the solid tumor (white arrow) and 2 vessels (black arrow) were found increased. This result is also in line with the anatomical structure of the CAM breast cancer cell xenograft, which has been demonstrated by Gadolinium CA distribution results before.

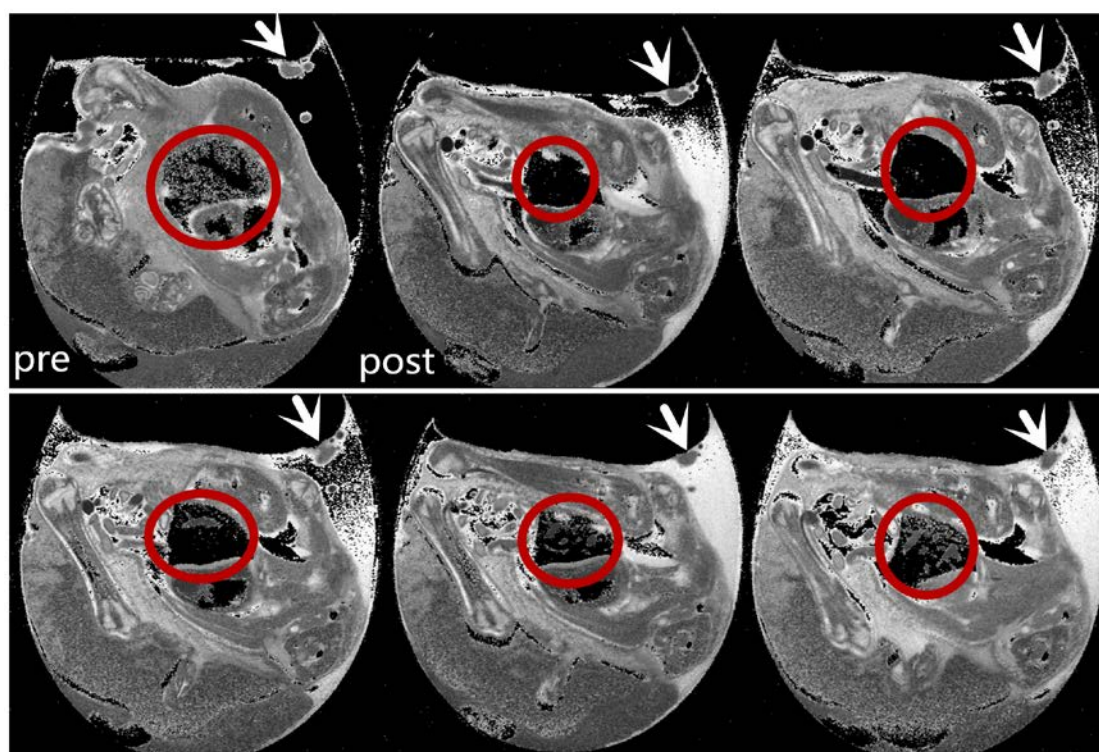


Figure 27: USPIO (Feraspin™ XS) bio-distribution assessment in ovo. In liver part (red circles) T<sub>2</sub> decreased after injection and recovered gradually. There was no obvious change in tumor area (white arrow).



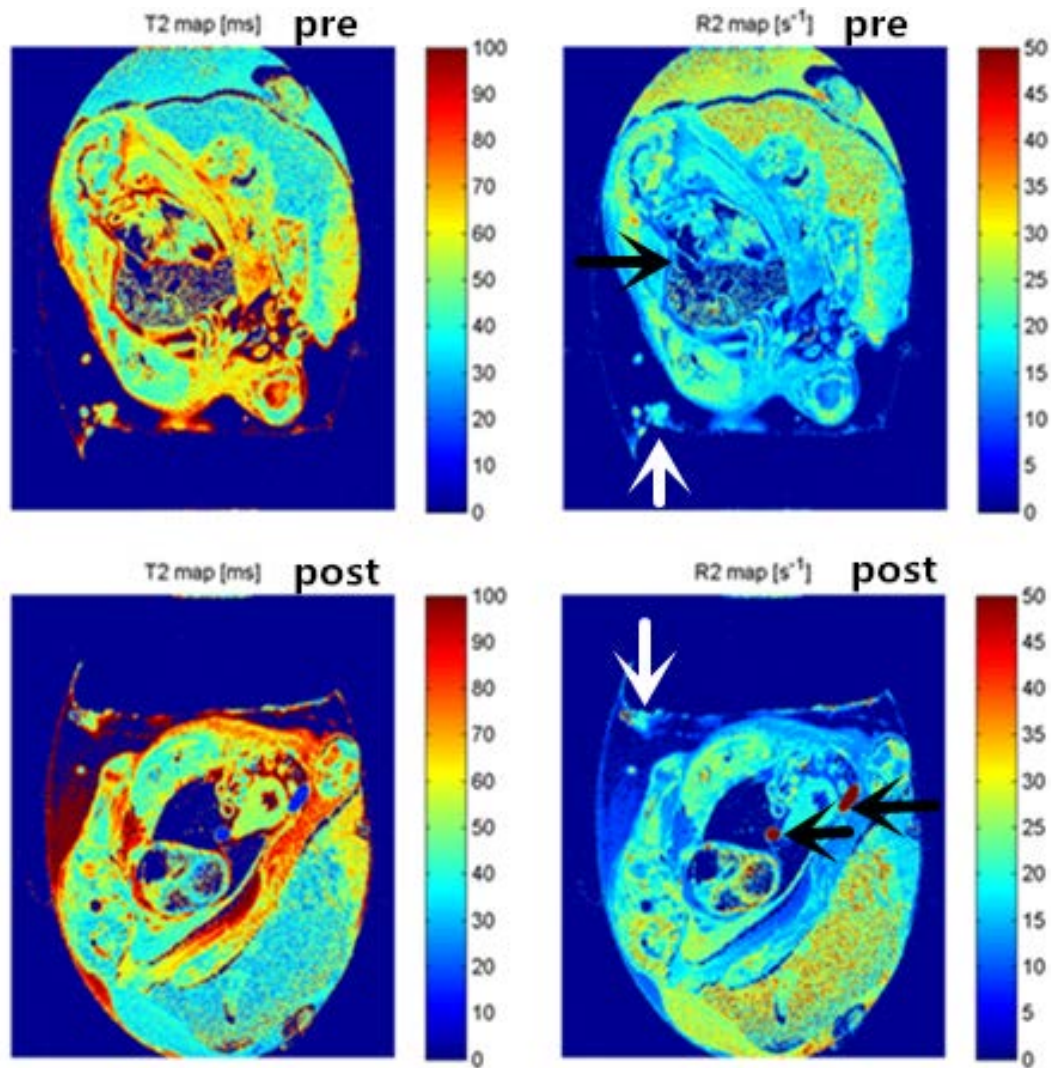


Figure 28: R<sub>2</sub> map images were shown in the right vertical. After USPIO intravascular injected into chicken embryo, the R<sub>2</sub> values of an area in the outmost part of solid tumor (white arrow) and 2 vessels (black arrow) were found increased.

## **4 Discussion**

### **4.1 CAM model – an alternative option for cancer xenograft research**

Appropriate tumor model is a prerequisite for cancer xenograft research. It is crucial for investigating the response to therapeutic interventions. Currently, the subcutaneous transplant models of athymic nude mice as well as nude rats represent the gold standard for in vivo investigations in tumor research. Such models allow grafting of xenografts due to the marked immunodeficiency of the animals. However, immune-deficient mouse or rat models have many significant disadvantages. Experiments using murine model in some fields for example in MRI research with conventional small animal imaging systems carry a high risk of contamination and animal infection, which may influence the results and limit longitudinal studies. In addition, use of nude murine for research is expensive and requires lengthy approval by the authorities. Thus, also according to the increasing demand to decrease or even prevent animal testing, the chorioallantoic membrane of fertilized chicken eggs has been established as an in vivo model for short-term investigations in cancer xenograft research. Chicken embryo system with chorioallantoic membrane is an important alternative option for cancer xenograft research. The use of this model as alternative model for tumor growth studies has been reported as an alternative simplified in vivo model (Syrovets et al. 2005). It provides rapid results and may be used as a simple inexpensive method practicable in any laboratory. Last but not least, the anticancer efficacies of chemotherapeutic drugs correlate well between CAM and mouse cancer models (Syrovets et al. 2005; Vogler et al. 2008).

Actually, this model possesses a lot of advantages and has long been underestimated. The system is naturally immune-deficient and may accept xenotransplants of various cancer cell lines. During early period of hatching the developing chick embryo is lacking in B and T-cell mediated immune function (Janse and Jeurissen 1991b). Therefore, this system enables the transplantation of heterogeneous systems or xenografts because graft rejection does not occur. Moreover, another distinct

advantage of using chick embryos is that chicken embryos are considered as an intermediate stage between isolated cultured cells and animal experiments, the chorioallantoic membrane model system is a borderline model between in vivo and in vitro system that does not raise ethical or legal problems, or violate animal protection laws. The usage of the in ovo tumor model is also well in line with the demand for a decrease of animal experiments with mammals. In addition, the chorioallantoic membrane is a temporary structure that exists only during the time of incubation. Like the mammalian placenta, the extraembryonic vessel system of the chorioallantoic membrane is not innervated. Unwanted animal stress factors such as transportation, operation, and impacts from the environments do not influence the experimental results. Furthermore, the chorioallantoic membrane contains a blood vessel network providing an excellent basis for primary tumor formation and a large source for angiogenic blood vessels. Thus, the CAM model may be applied to a variety of applications in tumor research and it is obviously well suited to replace at least parts of the conventional in vivo studies.

Because the potential and the increasing demands of CAM model in many research fields, the non-invasive imaging of chick embryos is getting more and more important. In most in ovo MRI studies reported so far, the in-plane resolution was limited to the order of  $200 \times 200 \mu\text{m}^2$  or even lower (Peebles et al. 2003; Holmes et al. 2008; Holmes et al. 2009; Bain et al. 2007; Xu et al. 2012; Boss et al. 2008; Zhou et al. 2012). This restriction was mainly caused by the limitations of scan time due to the rather short immobilization periods of the chick embryos. Higher resolution scans were mainly limited to ex vivo studies (B Hogers et al. 2001; Zhang, T Mesud Yelbuz, et al. 2003; Sawamura, Takahashi, Kathryn J McCarthy, et al. 2006; Seth W Ruffins et al. 2007; Goodall, Kisiwa, Prashar, Faulkner, Tokarczuk, Singh, Jonathan T Erichsen, et al. 2009) and could not be applied to longitudinal investigations.

Considering the tiny initial volumes of the grafted tumor and its often irregular shape and heterogeneity, for early tumor assessment and characterization, and especially

for longitudinal monitoring of tumor growth for sensitive identification of growth changes due to therapeutic interventions, high spatial resolutions are required.

Repeated pre-cooling has been proven not to slow down or arrest the development of the chicks by Maureen M. Bain et al (Bain et al. 2007). All of treated eggs hatched on the supposed day. Age-adapted precooling was first proposed by Hogers et al (Hogers et al. 2009) for imaging of quail embryos. The suggested precooling of the embryos at room temperature was limited to immobilization of the embryo till d11 after incubation with required cooling times beyond 200 minutes. For monitoring cancer growth, imaging has to be performed at later development stages of the embryo, which could not be realized with the room temperature protocol. With the suggested age-adapted cooling regime at 4°C, the feasibility of high-resolution in ovo MRI over the entire development cycle could be proven. Measurement of tumor size was possible as early as 96 h after cancer cell grafting, and growth of the tumor could be well assessed and measured on a daily basis till d16 after incubation.

In the MR scanning progress, the extra combined utilization of gaseous isoflurane could effectively extend the motion-artifact-free time even to 3 hours. Isoflurane is a volatile anesthetic widely used in veterinary anesthesia (Chapon et al. 2009). Based on observations of Alexander Heidrich et al (Heidrich et al. 2011) of hemodynamic effects of Isoflurane, UC anesthetic and Avertin on chick embryos, and also the experience of Andreas Boss et al of using Ketamin (Boss et al. 2008), various kinds of anesthetics for chicken embryo immobilization in ovo were tested. It turned out that without sufficient pre-cooling, anesthetics did not really work. But in combination with precooling, application of isoflurane could extend the immobilization time effectively. Even though, the combined protocol was tolerated by the chicken embryos, possible influences on embryo hatching still needs to be investigated. Isoflurane is a very short acting anesthetic, continuous supply during image acquisition exceeding 90 minutes was required. In conclusion, for MRI scan with acquisition time less than 90 minutes, age-adapted pre-cooling is sufficient for



immobilization. If longer scanning time is needed, combined utilization with high concentration but low flow rate isoflurane is recommended.

## **4.2 MRI imaging for CAM model**

### **4.2.1 Assessment of the morphology of chicken embryos and cancer cell xenografts on the CAM**

The comparison with histology revealed a good agreement between the non-invasive MRI method regarding shape and structure of the tumor. Parts of the tumor core poorly connected to the egg's blood system and characterized by low proliferation and angiogenesis, appears with reduced MR signal intensity in T<sub>2</sub>w images. Tumor edges exhibit higher MRI signals and are characterized by high density of blood vessels, increased cell mass and proliferation. Whether this is caused by the higher nuclei density or, more likely, by the blood volume remains to be clarified in future experiments. However, there is strong evidence that applying MRI may provide more than just the anatomical growth of the tumor.

The observed difference between the MRI-derived volume of the tumor and its weight might be attributed to the still limited spatial resolution of the MR images, some uniform weight loss caused by formalin fixation for more than 48 h (Mason, Lewis, and Weber 1983), or remains of the embedded Matrigel material requiring further investigation. The method enables the monitoring of chick embryo development and thus, may be applied to identify possible side effects of experimental therapies.

### **4.2.2 T<sub>2</sub> mapping and DWI application on CAM model**

MRI is not limited to imaging anatomy and dedicated technique as diffusion weighted imaging (DWI), T<sub>2</sub> mapping, perfusion imaging may further facilitate characterization and monitoring of the embryo and the tumor beyond simple assessment of volume and shape.

Characterization of embryonic tissue and cancer cell xenograft is an important topic in the field of regenerative medicine, stem cell and tumor research. The total amount

of water inside the avian egg at any time during development of the embryo depends on both the loss of water by diffusion through pores in the shell and the production of metabolic water through oxidation of yolk lipids (Ar and Rahn 1980; Paganelli 1980). A previous investigation in yolk of hen eggs did not reveal any change in the MR relaxation rates during the first days of incubation (i.e., up to day 4 of incubation) (Klammler and Kimmich 1990),  $T_2$  value kept the constant around 0.03s before the first 96h of incubation.

Andreas Boss et al measured  $T_1$ ,  $T_2$ , and magnetization transfer properties of brain, heart and liver of chicken embryos at day 5, 8, 11, 16 of embryonic incubation time at a 7 Tesla small animal MRI scanner. In their study, the  $T_1$  and  $T_2$  relaxation times measured in embryonic tissue decreased during embryonic development. The pattern of the relaxation rates probably reflected a decline in the relative free water content of the tissues with highest water content in the brain, intermediate water content in muscle tissue, and lowest water content in liver tissue.

In the present study, we showed MR relaxation rates of cancer cell xenograft as well as albumen and yolk of embryos at day 16 of incubation. The high field strength of 11.7T offers sufficient signal for MR imaging of tumor and embryos at day 16 of incubation.  $T_2$  quantification revealed good reproducibility of the  $T_2$  values (tumor =  $48 \pm 2.8$  ms, albumen =  $18 \pm 2.7$  ms, yolk =  $19.6 \pm 2.7$  ms). MR-relaxometry may become noninvasive tools for monitoring of tumor and tissue development in CAM models.

#### **4.2.3 CA assessment in CAM system**

##### **4.2.3.1 Commercial Gd CA assessment**

Assessment of the bio-distribution of MR contrast agents, and labelled pharmaceuticals after systemic injection was also investigated in this project.

Intravascular injection techniques have long been used in CAM system mainly for perfusion with fixatives (Zhang, T. Mesud Yelbuz, et al. 2003; B. Hogers et al. 2001)

and assessment of anti-cancer medicines (Morad et al. 2011), but never for MR contrast agent bio-distribution assessment to our knowledge.

The optimal CA dosage suitable for chick embryos was investigated. Chick embryos at day 16 of incubation were used for assessment because during that day the blood volume of chicken embryo has developed to the peak value during the whole incubation period. The mean reported blood volume is 3.13 ml (Kind 1975). Vasovist was chosen as representative Gd CA for dosage assessment. As a clinical commercial blood-pool MR contrast agent, it has several advantages. It consists of a low molecular weight molecule chelated to Gadolinium that strongly binds with the plasma proteins, leading to the contrast agent remaining intravascular for longer periods so that the imaging window after administration is about 30–60 min for patient application (Hartmann et al. 2006; Goyen, Shamsi, and Schoenberg 2006). The recommended dosage for patients is 0.12 ml/kg while the blood volume of adult human being is 70-80 ml/kg. So the recommended rate of Vasovist/blood volume for human is 0.15%-0.17%. As mentioned before, blood volume of chicken embryo at day 16 of incubation is around 3 ml (Kind 1975). According to the recommended rate for human, the recommended Vasovist dosage for chicken embryo at day 16 of incubation is roughly 5  $\mu$ l. But after injection of 5 $\mu$ l Vasovist for chicken embryo model, there was no satisfactory enhancement produced. Specific dosage value suitable for chicken embryo was needed. 8 chicken embryos were used for testing different Vasovist dosages (5, 10, 20, 50, 60, 70, 80, and 90  $\mu$ L). The SNR kept rising with increased Vasovist dosage till administration of 80  $\mu$ l. After SNR calculation and image comparison, 80  $\mu$ l was confirmed as most suitable Vasovist dosage for chicken embryos at day 16 of incubation.

Differences between Vasovist, Dotarem and Multihance were investigated. After the management of the same Gd concentration, Vasovist was found to produce better enhancement than Multihance. For Dotarem, from 16 hours after injection the gizzard and cloaca of chicken embryo was found to be enhanced by contrast agent

which was not supposed to happen. This kind of situation did not happen in the chicken embryos after injection of Vasovist and Multihance. The reason still needs to be figured out in further experiments. For the reason of efficiency and embryo safety, Vasovist was confirmed as recommended commercial Gd contrast agent.

Optimal timing for maximal contrast enhancement was investigated for blood pool and liver parenchyma when for clinical application the imaging window after Vasovist administration is about 30–60 min (Hartmann et al. 2006; Goyen, Shamsi, and Schoenberg 2006). But in chicken embryo 30 minutes was identified as peak time point for blood pool and 3 hours for liver parenchyma.

Systematic assessment of Vasovist bio-distribution in 10 chicken embryos at day 16 of incubation was investigated. Time-SNR curve for blood pool, liver parenchyma brain, and allantoic fluid before and at 0.5, 3, 5, 20, 40 hours post-injection were analyzed. Most organs of embryos were enhanced during the first 5 hours. Slight enhancement was even observed in the brain likely due to the immature developed blood-brain barrier. After 20 hours, CA was gradually metabolized into allantoic fluid. The whole CA bio-distribution was described in detail.

After bio-distribution was successfully assessed in normal chicken embryos, the same protocol was also used for cancer cell xenograft assessment. Micro structures with many details of tiny tumor were shown in different contrast which presented unique information for the first time. In conclusion, the Vasovist accumulated mainly in the surrounding area of tumor which is closely attached and connected to the CAM and full of vessels. Further enhancement was observed in the center part of solid tumor with low cell density.

#### **4.2.3.2 Novel Gd conjugated PbP assessment in ovo**

As potential application of the in ovo model, is the assessment of bio-distribution of novel CA. As an example for a new CA, Gd conjugated PbP - cHSA-PEO(2000)<sub>16</sub>-Gd-DOX<sub>27</sub> was investigated. cHSA-PEO(2000)<sub>16</sub>-Gd-DOX<sub>27</sub> is based on the backbone of poly-cationic serum albumin, which has exhibited an improved

cell and tissue uptake efficiency as demonstrated in previous studies (Kumagai, Eisenberg, and Pardridge 1987). In order to address high blood circulation as well as low immunogenicity already at an early stage, a very high degree of pegylation is subsequently implemented to efficiently shield potential epitopes at the albumin surface. Pegylation represents a well-elaborated strategy tested in clinical trials to prolong the circulation time of protein therapeutics and minimize their immunogenicity (Jevsevar, Kunstelj, and Porekar 2010). In addition, PEO brush architectures of polymersomes have shown greatly improved blood circulation compared with pegylated liposomes (Photos et al. 2003).

Compared to the  $r_1$  relaxivity of clinically used Gd contrast agents of Gd-DOTA ( $4.3 \text{ mM}^{-1}\text{s}^{-1}$ ) and Gd-DTPA ( $4.5 \text{ mM}^{-1}\text{s}^{-1}$ ), the polymeric Gd micelles exhibited significantly better enhancement indicating higher sensitivity. Compared to other gadolinium-based macromolecular contrast agents reported previously, the paramagnetic properties of cHSA-PEO(2000)<sub>16</sub>-Gd-DOX<sub>27</sub> showed comparable relaxivity.

Assessment of the bio-distribution proved specific accumulation of the CA in the cancer cell xenografts for at least 10 hours. In contrast, Multihance did not show substantial enhancement with similar Gd-concentration.

Thus, the novel micelles overcome the intrinsic limitation associated with small molecule  $\text{Gd}^{3+}$  complexes, regarding low relaxivity and unspecific tissue uptake. It has been proven as a reliable and reproducible MR contrast agent for breast cancer xenograft imaging in ovo.

#### **4.2.3.3 USPIO assessment in ovo**

Iron-oxide based contrast agents also play an important role in MRI. Aside the specific binding affinity, drug targeting is based on a passive accumulation mechanism that is controlled by particle size and surface characteristics of the colloids. Particles ranging in size below 300 nm accumulate in solid tumors due to the enhanced permeability and retention effect (Wacker 2013). While circulating through

the blood stream, these CA undergoes an opsonization by the immune system followed by endocytosis into macrophages. Particles of greater diameters are rapidly cleared from the plasma and smaller colloidal carriers are eliminated through the kidney. With increasing circulation time, the extent of passive accumulation into the target tissue increases significantly.

Ferapin XS with the size of 10-20 nm was also assessed of bio-distribution in breast cancer xenograft on CAM. After USPIO injected intravascular, it is very obvious that relaxivity in liver area was markedly decreased and after 5 hours relaxivity started to recover. Similar effect could also be observed in part of surrounding tumor area in reverted  $R_2$  maps.  $R_2$  value of a part surrounding tumor area was increased obviously after CA injection. As our experience, the area should be loose tissue surrounding the solid tumor.

## 5 Summary

The chick chorioallantoic membrane model has been successfully used to study angiogenesis, cancer progression and its pharmacological treatment, tumor pharmacokinetics, and properties of novel nanomaterials. Magnetic resonance imaging is an attractive technique for non-invasive and longitudinal monitoring of physiological processes and tumor growth.

In this thesis an age-adapted cooling regime for immobilization of the chick embryo is proposed. In combination with gaseous isoflurane anesthesia scan time of up to 3 hours could be realized in ovo. Reliable immobilization completely avoided motion artifacts, enabling high resolution MR imaging of the chicken embryo and also tumor xenograft on the chorioallantoic membrane with different contrasts.

Tumor growth monitoring was firstly evaluated after xenotransplantation of human MDA-MB-231 breast cancer cells on the chorioallantoic membrane. Tumor volumes were monitored from day 4 to day 9 after grafting (day 11 to day 16 after incubation) applying a  $T_2$ -weighted multislice rapid acquisition with relaxation enhancement sequence. Excellent anatomical details could be obtained in the embryo and tumors. Tumor volumes could be quantified over time. At day 9 after grafting, the tumors were collected and compared with the magnetic resonance imaging-derived data by histology and weight measurements. Data correlated very well.

Diffusion weighted imaging and  $T_2$  mapping were also tested at day 9 after grafting in chicken embryos.  $T_2$  values of solid tumor have been calculated, which could be taken as the reference for further investigation on novel anti-cancer therapy assessment.

Magnetic resonance contrast agents were also assessed for bio-distribution in the chorioallantoic membrane model. 80  $\mu$ l Vasovist was used for assessment at 30 minutes, 3, 5, 20 and 40 hours post-injection in ovo. Main vessels showed maximal enhancement at 30 minutes post-injection, while liver parenchyma showed delayed enhancement after 3 hours. After 20 hours, most of contrast agent was translated to the allantoic fluid. In tumors the main enhancement was observed in the area

surrounding the solid tumor and in the center part, corresponding to the low cell density, which was proved by immune-histology analysis and acknowledged us better about anatomical structures of breast cancer xenograft.

Novel gadolinium conjugated micelles  $\text{cHSA-PEO}(2000)_{16}\text{-Gd-DOX}_{27}$  were evaluated in ovo. After relaxivity measurement, micelles of 3.6 mM gadolinium concentration were intravascular injected in ovo. Accumulation of the micelles was specifically observed in the tumor tissues with persistent enhancement for more than 10 hours.

To the best of our knowledge, this is the first report on monitoring breast cancer tumor growth by magnetic resonance imaging also assess contrast agents bio-distribution in a chorioallantoic membrane model in ovo. The results prove the feasibility of high-resolution magnetic resonance imaging for longitudinal tumor and organ growth monitoring, and also possess the potential utility for assess novel micelles. The suggested method is promising for future applications such as testing tailored and/or targeted treatment strategies, longitudinal monitoring of tumor development, analysis of therapeutic efficacies of drugs, or assessment of tumor pharmacokinetics. The method provides an alternative to animal experimentation.

In conclusion, the work proved the principal application of magnetic resonance imaging for high-fidelity in ovo imaging with the potential of using this approach for initial assessment of the bio-distribution of novel contrast agents.



## 6 Reference

Achenbach, M., Figiel, J. H., Burbelko, M. & Heverhagen, J. T. Prospective comparison of image quality and diagnostic accuracy of 0.5 molar gadobenate dimeglumine and 1.0 molar gadobutrol in contrast-enhanced run-off magnetic resonance angiography of the lower extremities. *J. Magn. Reson. Imaging* 32, 1166–1171 (2010).

Ar, A. & Rahn, H. Water in the Avian Egg Overall Budget of Incubation. *Integr. Comp. Biol.* 20, 373–384 (1980).

Aristotle. *Historia Animalium*. II, Harvard University Press; Loeb Library Edition edition (1970).

Armstrong, P. B., Quigley, J. P. & Sidebottom, E. Transepithelial invasion and intramesenchymal infiltration of the chick embryo chorioallantois by tumor cell lines. *Cancer Res.* 42, 1826–1837 (1982).

Bain MM, Fagan AJ, Mullin JM, McNaught I, McLean J, Condon B. Noninvasive monitoring of chick development in ovo using a 7T MRI system from day 12 of incubation through to hatching. *J. Magn. Reson. Imaging* 26, 198–201 (2007).

Boss A, Oppitz M, Wehrl HF, Rossi C, Feuerstein M, Claussen CD, Drews U, Pichler BJ, Schick F. Measurement of T1, T2, and Magnetization Transfer Properties during Embryonic Development at 7 Tesla Using the Chicken Model. *Journal of Magnetic Resonance Imaging* 28(6): 1510–1514 (2008).

Bottrill, M., Kwok, L. & Long, N. J. Lanthanides in magnetic resonance imaging. *Chem. Soc. Rev.* 35, 557 (2006).

Büchele B, Zugmaier W, Estrada A, Genze F, Syrovets T, Paetz C, Schneider B, Simmet T. Characterization of 3 $\alpha$ -acetyl-11-keto- $\alpha$ -boswellic acid, a pentacyclic triterpenoid inducing apoptosis in vitro and in vivo. *Planta Med.* 72, 1285–1289 (2006).

Büchele, B., Zugmaier, W., Genze, F. & Simmet, T. High-performance liquid chromatographic determination of acetyl-11-keto- $\alpha$ -boswellic acid, a novel pentacyclic triterpenoid, in plasma using a fluorinated stationary phase and photodiode array detection: application in pharmacokinetic studies. *J. Chromatogr. B Analyt. Technol. Biomed. Life Sci.* 829, 144–148 (2005).

Bui T, Stevenson J, Hoekman J, Zhang S, Maravilla K, Ho RJ. Novel Gd

nanoparticles enhance vascular contrast for high-resolution magnetic resonance imaging. *PLoS One* 5, (2010).

Burkhardt, A., Meister, S., Bergmann, R. & Koch, E. Influence of storage on the position of the germinal disc in the fertilized unincubated chicken egg. *Poult. Sci.* 90, 2169–2173 (2011).

Caravan, P., Ellison, J. J., McMurry, T. J. & Lauffer, R. B. Gadolinium(III) Chelates as MRI Contrast Agents: Structure, Dynamics, and Applications. *Chem. Rev.* 99, 2293–2352 (1999).

Chapon C, Jackson JS, Aboagye EO, Herlihy AH, Jones WA, Bhakoo KK. An in vivo multimodal imaging study using MRI and PET of stem cell transplantation after myocardial infarction in rats. *Mol. Imaging Biol.* 11, 31–38 (2009)

Chawla S, Kim S, Dougherty L, Wang S, Loevner LA, Quon H, Poptani H. Pretreatment diffusion-weighted and dynamic contrast-enhanced MRI for prediction of local treatment response in squamous cell carcinomas of the head and neck. *AJR Am. J. Roentgenol.* 200, 35–43 (2013).

Cheng, Z., Thorek, D. L. J. & Tsourkas, A. Gadolinium-Conjugated Dendrimer Nanoclusters as a Tumor-Targeted T1 Magnetic Resonance Imaging Contrast Agent. *Angew. Chem. Int. Ed. Engl.* 49, 346–350 (2010).

Deryugina, E. I. & Quigley, J. P. Chick embryo chorioallantoic membrane model systems to study and visualize human tumor cell metastasis. *Histochem. Cell Biol.* 130, 1119–1130 (2008).

Ellingson BM, Cloughesy TF, Lai A, Nghiemphu PL, Lalezari S, Zaw T, Motevalibashinaeini K, Mischel PS, Pope WB. Quantification of edema reduction using differential quantitative T2 (DQT2) relaxometry mapping in recurrent glioblastoma treated with bevacizumab. *J. Neurooncol.* 106, 111–119 (2012).

Estrada AC, Syrovets T, Pitterle K, Lunov O, Büchele B, Schimana-Pfeifer J, Schmidt T, Morad SA, Simmet T. Tirucallic acids are novel pleckstrin homology domain-dependent Akt inhibitors inducing apoptosis in prostate cancer cells. *Mol. Pharmacol.* 77, 378–387 (2010).

Gerretsen SC, le Maire TF, Miller S, Thurnher SA, Herborn CU, Michaely HJ, Kramer H, Vanzulli A, Vymazal J, Wasser MN, Ballarati CE, Kirchin MA, Pirovano G, Leiner T. Multicenter, double-blind, randomized, intraindividual crossover

comparison of gadobenate dimeglumine and gadopentetate dimeglumine for MR angiography of peripheral arteries. *Radiology* 255, 988–1000 (2010).

Gerstner, E. R., Sorensen, A. G., Jain, R. K. & Batchelor, T. T. Advances in neuroimaging techniques for the evaluation of tumor growth, vascular permeability, and angiogenesis in gliomas. *Curr. Opin. Neurol.* 21, 728–735 (2008).

Giesel FL, von Tengg-Kobligk H, Wilkinson ID, Siegler P, von der Lieth CW, Frank M, Lodemann KP, Essig M. Influence of human serum albumin on longitudinal and transverse relaxation rates ( $r_1$  and  $r_2$ ) of magnetic resonance contrast agents. *Invest. Radiol.* 41, 222–228 (2006).

Glover, J. C., Boulland, J.-L., Halasi, G. & Kasumacic, N. Chimeric animal models in human stem cell biology. *ILAR J.* 51, 62–73 (2009).

Goodall N, Kisiswa L, Prashar A, Faulkner S, Tokarczuk P, Singh K, Erichsen JT, Guggenheim J, Halfter W, Wride MA. 3-Dimensional modelling of chick embryo eye development and growth using high resolution magnetic resonance imaging. *Exp. Eye Res.* 89, 511–521 (2009).

Goyen, M. Gadofosveset-enhanced magnetic resonance angiography. *Vasc. Health Risk Manag.* 4, 1–9 (2008).

Goyen, M., Shamsi, K. & Schoenberg, S. O. Vasovist-enhanced MR angiography. *Eur. Radiol.* 16 Suppl 2, B9–14 (2006).

Hamburger, V. & Hamilton, H. L. A series of normal stages in the development of the chick embryo. *J. Morphol.* 88, 49–92 (1951).

Härtl, A., Sauerbrei, A., Stelzner, A. & Wutzler, P. Influenza infection of the embryonated hen's egg/an alternative model for in vivo evaluation of antiviral compounds. *Arzneimittelforschung.* 54, 130–134 (2004).

Hartmann, M., Wiethoff, A. J., Hentrich, H.-R. & Rohrer, M. Initial imaging recommendations for Vasovist angiography. *Eur. Radiol.* 16 Suppl 2, B15–23 (2006).

Hatakenaka M, Soeda H, Yabuuchi H, Matsuo Y, Kamitani T, Oda Y, Tsuneyoshi M, Honda H. Apparent diffusion coefficients of breast tumors: clinical application. *Magn. Reson. Med.* 7, 23–29 (2008).

Heidrich, A., Würbach, L., Opfermann, T. & Saluz, H. P. Motion-Artifact-Free In

Vivo Imaging Utilizing Narcotized Avian Embryos In Ovo. *Mol. Imaging Biol.* 13, 208–214 (2011).

Herborn CU, Honold E, Wolf M, Kemper J, Kinner S, Adam G, Barkhausen J. Clinical Safety and Diagnostic Value of the Gadolinium Chelate Gadoterate Meglumine (Gd-DOTA): *Invest. Radiol.* 42, 58–62 (2007).

Higgins, D. & Pappano, A. J. Development of transmitter secretory mechanisms by adrenergic neurons in the embryonic chick heart ventricle. *Dev. Biol.* 87, 148–162 (1981).

Hoehn-Berlage, M., Tolxdorff, T., Bockhorst, K., Okada, Y. & Ernestus, R. I. In vivo NMR T2 relaxation of experimental brain tumors in the cat: a multiparameter tissue characterization. *Magn. Reson. Imaging* 10, 935–947 (1992).

Hogers B, Gross D, Lehmann V, de Groot HJ, de Roos A, Gittenberger-de Groot AC, Poelmann RE. Magnetic resonance microscopy at 17.6-Tesla on chicken embryos in vitro. *J. Magn. Reson. Imaging* 14, 83–86 (2001).

Hogers B, van der Weerd L, Olofsen H, van der Graaf LM, DeRuiter MC, Gittenberger-de Groot AC, Poelmann R. Non-invasive tracking of avian development in vivo by MRI. *NMR Biomed.* 22, 365–373 (2009).

Holmes, W. M., McCabe, C., Mullin, J. M., Condon, B. & Bain, M. M. Images in cardiovascular medicine. Noninvasive self-gated magnetic resonance cardiac imaging of developing chick embryos in ovo. *Circulation* 117, e346–347 (2008).

Holmes, W. M., McCabe, C., Mullin, J. M., Condon, B. & Bain, M. M. In ovo non-invasive quantification of the myocardial function and mass of chick embryos using magnetic resonance imaging. *NMR Biomed.* 22, 745–752 (2009).

Janse, E. M. & Jeurissen, S. H. Ontogeny and function of two non-lymphoid cell populations in the chicken embryo. *Immunobiology* 182, 472–481 (1991).

Jevsevar, S., Kunstelj, M. & Porekar, V. G. PEGylation of therapeutic proteins. *Biotechnol. J.* 5, 113–128 (2010).

Kaufman, N., Kinney, T. D., Mason, E. J. & Prieto, L. C. Maintenance of human neoplasm on the chick chorioallantoic membrane. *Am. J. Pathol.* 32, 271–285 (1956).

Kind, C. The development of the circulating blood volume of the chick embryo. *Anat. Embryol. (Berl.)* 147, 127–132 (1975).

King AD, Mo FK, Yu KH, Yeung DK, Zhou H, Bhatia KS, Tse GM, Vlantis AC, Wong JK, Ahuja AT. Squamous cell carcinoma of the head and neck: diffusion-weighted MR imaging for prediction and monitoring of treatment response. *Eur. Radiol.* 20, 2213–2220 (2010).

Klammler, F. & Kimmich, R. Volume-selective and spectroscopically resolved NMR investigation of diffusion and relaxation in fertilised hen eggs. *Phys. Med. Biol.* 35, 67–79 (1990).

Koop S, MacDonald IC, Luzzi K, Schmidt EE, Morris VL, Grattan M, Khokha R, Chambers AF, Groom AC. Fate of melanoma cells entering the microcirculation: over 80% survive and extravasate. *Cancer Res.* 55, 2520–2523 (1995).

Kumagai, A. K., Eisenberg, J. B. & Pardridge, W. M. Absorptive-mediated endocytosis of cationized albumin and a beta-endorphin-cationized albumin chimeric peptide by isolated brain capillaries. Model system of blood-brain barrier transport. *J. Biol. Chem.* 262, 15214–15219 (1987).

Le Noble FA, Schreurs NH, van Straaten HW, Slaaf DW, Smits JF, Rogg H, Struijker-Boudier HA. Evidence for a novel angiotensin II receptor involved in angiogenesis in chick embryo chorioallantoic membrane. *Am. J. Physiol.* 264, R460–465 (1993).

Leach MO, Brindle KM, Evelhoch JL, Griffiths JR, Horsman MR, Jackson A, Jayson G, Judson IR, Knopp MV, Maxwell RJ, McIntyre D, Padhani AR, Price P, Rathbone R, Rustin G, Tofts PS, Tozer GM, Vennart W, Waterton JC, Williams SR, Workman P. Assessment of antiangiogenic and antivascular therapeutics using MRI: recommendations for appropriate methodology for clinical trials. *Br. J. Radiol.* 76 Spec No 1, S87–91 (2003).

Leng T, Miller JM, Bilbao KV, Palanker DV, Huie P, Blumenkranz MS. The chick chorioallantoic membrane as a model tissue for surgical retinal research and simulation. *Retina* 24, 427–434 (2004).

Loos C, Syrovets T, Musyanovych A, Mailänder V, Landfester K, Simmet T. Amino-functionalized nanoparticles as inhibitors of mTOR and inducers of cell cycle arrest in leukemia cells. *Biomaterials* 35, 1944–1953 (2014).

Lunov O, Syrovets T, Loos C, Beil J, Delacher M, Tron K, Nienhaus GU, Musyanovych A, Mailänder V, Landfester K, Simmet T. Differential uptake of

functionalized polystyrene nanoparticles by human macrophages and a monocytic cell line. *ACS Nano* 5, 1657–1669 (2011).

Mason, W. T., Lewis, P. A. & Weber, C. I. An evaluation of benthic macroinvertebrate biomass methodology : Part 1. Laboratory analytical methods. *Environ. Monit. Assess.* 3, 29–44 (1983).

Merbach, André, Lothar Helm, and Éva Tóth, eds. *The Chemistry of Contrast Agents in Medical Magnetic Resonance Imaging. In The Chemistry of Contrast Agents in Medical Magnetic Resonance Imaging* Pp. i–xvi. Chichester, UK: John Wiley & Sons, Ltd. <http://doi.wiley.com/10.1002/9781118503652.fmatter>, accessed January 12, 2015.

Morad SA, Schmid M, Büchele B, Siehl HU, El Gafaary M, Lunov O, Syrovets T, Simmet T. A novel semisynthetic inhibitor of the FRB domain of mammalian target of rapamycin blocks proliferation and triggers apoptosis in chemoresistant prostate cancer cells. *Mol. Pharmacol.* 83, 531–541 (2013).

Morad SA, Schmidt C, Büchele B, Schneider B, Wenzler M, Syrovets T, Simmet T. (8R)-3 $\beta$ ,8-dihydroxypolypoda-13E,17E,21-triene induces cell cycle arrest and apoptosis in treatment-resistant prostate cancer cells. *J. Nat. Prod.* 74, 1731–1736 (2011).

Morgan D, Diamond DM, Gottschall PE, Ugen KE, Dickey C, Hardy J, Duff K, Jantzen P, DiCarlo G, Wilcock D, Connor K, Hatcher J, Hope C, Gordon M, Arendash GW. A beta peptide vaccination prevents memory loss in an animal model of Alzheimer's disease. *Nature* 408, 982–985 (2000).

Neumann E, Frei E, Funk D, Becker MD, Schrenk HH, Müller-Ladner U, Fiehn C. Native albumin for targeted drug delivery. *Expert Opin. Drug Deliv.* 7, 915–925 (2010).

Oh J, Cha S, Aiken AH, Han ET, Crane JC, Stainsby JA, Wright GA, Dillon WP, Nelson SJ. Quantitative apparent diffusion coefficients and T2 relaxation times in characterizing contrast enhancing brain tumors and regions of peritumoral edema. *J. Magn. Reson. Imaging* 21, 701–708 (2005).

Paganelli, C. V. *The Physics of Gas Exchange Across the Avian Eggshell. Integr. Comp. Biol.* 20, 329–338 (1980).

Partridge SC, Gibbs JE, Lu Y, Esserman LJ, Tripathy D, Wolverton DS, Rugo HS, Hwang ES, Ewing CA, Hylton NM. MRI measurements of breast tumor volume

predict response to neoadjuvant chemotherapy and recurrence-free survival. *AJR Am J Roentgenol.* 184, 1774–1781 (2005).

Peebles DM, Dixon JC, Thornton JS, Cady EB, Priest A, Miller SL, Blanco CE, Mulder TL, Ordidge RJ, Rodeck CH. Magnetic resonance proton spectroscopy and diffusion weighted imaging of chick embryo brain in ovo. *Brain Res. Dev. Brain Res.* 141, 101–107 (2003).

Photos, P. J., Bacakova, L., Discher, B., Bates, F. S. & Discher, D. E. Polymer vesicles in vivo: correlations with PEG molecular weight. *J. Control. Release* 90, 323–334 (2003).

Pintaske J, Martirosian P, Graf H, Erb G, Lodemann KP, Claussen CD, Schick F. Relaxivity of Gadopentetate Dimeglumine (Magnevist), Gadobutrol (Gadovist), and Gadobenate Dimeglumine (MultiHance) in human blood plasma at 0.2, 1.5, and 3 Tesla. *Invest. Radiol.* 41, 213–221 (2006).

Ribatti D, Nico B, Vacca A, Roncali L, Burri PH, Djonov V. Chorioallantoic membrane capillary bed: a useful target for studying angiogenesis and anti-angiogenesis in vivo. *Anat. Rec.* 264, 317–324 (2001).

Rohrer, M., Bauer, H., Mintorovitch, J., Requardt, M. & Weinmann, H.-J. Comparison of magnetic properties of MRI contrast media solutions at different magnetic field strengths. *Invest. Radiol.* 40, 715–724 (2005).

Ruffins SW, Martin M, Keough L, Truong S, Fraser SE, Jacobs RE, Lansford R. Digital three-dimensional atlas of quail development using high-resolution MRI. *ScientificWorldJournal* 7, 592–604 (2007).

Ruffins, Seth W, Melanie Martin, Lindsey Keough, et al.  
2007 Digital Three-Dimensional Atlas of Quail Development Using High-Resolution MRI. *TheScientificWorldJournal* 7: 592–604.

Sawamura C, Takahashi M, McCarthy KJ, Shen Z, Fukai N, Rodriguez EK, Snyder BD. Effect of in ovo immobilization on development of chick hind-limb articular cartilage: an evaluation using micro-MRI measurement of delayed gadolinium uptake. *Magn. Reson. Med.* 56, 1235–1241 (2006).

Sawamura C, Takahashi M, McCarthy KJ, Shen Z, Fukai N, Rodriguez EK, Snyder BD. Effect of in ovo immobilization on development of chick hind-limb articular cartilage: an evaluation using micro-MRI measurement of delayed gadolinium uptake. *Magn. Reson. Med.* 56, 1235–1241 (2006).

Strome, E. M. & Doudet, D. J. Animal models of neurodegenerative disease: insights from in vivo imaging studies. *Mol. Imaging Biol.* 9, 186–195 (2007).

Syrovets T, Gschwend JE, Büchele B, Laumonnier Y, Zugmaier W, Genze F, Simmet T. Inhibition of IkappaB kinase activity by acetyl-boswellic acids promotes apoptosis in androgen-independent PC-3 prostate cancer cells in vitro and in vivo. *J. Biol. Chem.* 280, 6170–6180 (2005).

Taber, L. A., Keller, B. B. & Clark, E. B. Cardiac mechanics in the stage-16 chick embryo. *J. Biomech. Eng.* 114, 427–434 (1992).

Tacar, O., Sriamornsak, P. & Dass, C. R. Doxorubicin: an update on anticancer molecular action, toxicity and novel drug delivery systems. *J. Pharm. Pharmacol.* 65, 157–170 (2013).

Vogler M, Walczak H, Stadel D, Haas TL, Genze F, Jovanovic M, Gschwend JE, Simmet T, Debatin KM, Fulda S. Targeting XIAP Bypasses Bcl-2-Mediated Resistance to TRAIL and Cooperates with TRAIL to Suppress Pancreatic Cancer Growth in Vitro and in Vivo. *Cancer Research* 68(19): 7956–7965 (2008).

Wacker, M. Nanocarriers for intravenous injection—The long hard road to the market. *Int. J. Pharm.* 457, 50–62 (2013).

Wang, J. P., Qi, L., Moore, M. R. & Ng, J. C. A review of animal models for the study of arsenic carcinogenesis. *Toxicol. Lett.* 133, 17–31 (2002).

Wu, Y. Polypeptide hybrid biomaterials developed from protein precursors - a novel strategy and biomedical applications: [D].Ulm: Universität Ulm, 2013.

Wu Y, Ihme S, Feuring-Buske M, Kuan SL, Eisele K, Lamla M, Wang Y, Buske C, Weil T. A Core-Shell Albumin Copolymer Nanotransporter for High Capacity Loading and Two-Step Release of Doxorubicin with Enhanced Anti-Leukemia Activity. *Adv. Healthc. Mater.* 2, 884–894 (2013).

Xu J, Delproposto Z, Zhou Z, Shen H, Xuan SY, Li QH, Haacke EM, Hu J. In Ovo Monitoring of Smooth Muscle Fiber Development in the Chick Embryo: Diffusion Tensor Imaging with Histologic Correlation. *PLoS ONE* 7, e34009 (2012).

Zhang X, Yelbuz TM, Cofer GP, Choma MA, Kirby ML, Johnson GA. Improved preparation of chick embryonic samples for magnetic resonance microscopy. *Magn. Reson. Med.* 49, 1192–1195 (2003).



Zhou Z, Xu J, Delproposto ZS, Hua J, Fan Y, Zhang Z, Ye Y, Haacke EM, Hu J. Feasibility of in ovo diffusion tractography in the chick embryo using a dual-cooling technique. *J. Magn. Reson. Imaging* 36, 993–1001 (2012).

Zhu L, van de Lavoie MC, Albanese J, Beenhouwer DO, Cardarelli PM, Cuisson S, Deng DF, Deshpande S, Diamond JH, Green L, Halk EL, Heyer BS, Kay RM, Kerchner A, Leighton PA, Mather CM, Morrison SL, Nikolov ZL, Passmore DB, Pradas-Monne A, Preston BT, Rangan VS, Shi M, Srinivasan M, White SG, Winters-Digiaccio P, Wong S, Zhou W, Etches RJ. Production of human monoclonal antibody in eggs of chimeric chickens. *Nat. Biotechnol.* 23, 1159–1169 (2005).

Zuo Z, Syrovets T, Genze F, Abaei A, Ma G, Simmet T, Rasche V. High-resolution MRI analysis of breast cancer xenograft on the chick chorioallantoic membrane. *NMR Biomed.* 28, 440–447 (2015).

## **7 Acknowledgments**

This doctoral thesis would not be possible without generous support kindly provided by a lot of people.

I owe my overwhelming thanks to my supervisor Professor Dr. rer. nat. Volker Rasche, the head of Experimental Cardiovascular Imaging, Core Facility Small Animal MRI of Ulm University, for his patient teaching and guidance leading me into MRI world, for his fully support encouraging me to submit abstract for conference and to get papers published, and also for his understanding when I face some situations and need to change my research plan.

I also owe thanks to Dr. Alireza Abaei, my colleague and best friend in Germany, whose help and support not only in the work but also in my life in Ulm. I have much enjoyed working together for the past years.

Thanks my colleague and friend Frau Anne Subgang who showed me the MR scanner operations, bought me experimental materials, translated letters written in German for me and also those relaxing talking from the very first day of my work in lab.

I am very grateful to Frau Felicitas Genze for providing me chicken embryos with tumor xenograft, teaching me intravascular injection technique in ovo and borrowing me incubator and lamp. Many thanks for Professor Dr. Tatiana Syrovets for providing us MDA-MB-231 cell lines. Thanks Alexander Pochert for always borrowing me pipettes and tips.

I extend my thanks to the colleagues, Michael Schöffler, Anna-Katinka Bracher, Ina Vernikouskaya, Jan Paul, Marta Tibiletti, Michael Eder and Stefan Wundrak for their friendly kindness and helps.

I also owe my deepest gratitude to Ma Gen-Shan, whose generous help and support benefits me much in my study, my future clinical and research work.

I always thank many Chinese friends for their friendship and support during my stay in Ulm. Thank you very much: Dr. Li Huang, Dr. Chunxiang Fan, Dr. Yan Wang, Shan-Hu

Qiu, Xue-Yao Ma, Wei-Na Liu, Jin-Jing Ren, Dr. Shaoxia Zhou, Han Yin, Dr. Jing Lu, Dr. Zhong-Ke Sun, and all the friends whose names are not listed here.

I offer my regards and blessings to all of those who supported me in any respect during the completion of my study.

Last but not least, special thanks to my wife and my parents for their endless support, understanding and encouragement which motivate and influence me forever. Without their support, it is not possible for me to go through the whole progress.

## 8 Curriculum vitae

### Personal Information

Name: Zhi  
Surname: Zuo  
Gender: Male  
Birth date: 05.01.1988  
Birthplace: Lian'shui, China  
Nationality: Chinese

### EDUCATION:

08/2013 – present    Experimental Cardiovascular Imaging, Core Facility Small Animal MRI, Ulm University, Ulm, Germany

*MD candidate, my focus was to investigate in Ovo MRI*

09/2010 – 07/2012    Medical College of Southeast University, Nanjing, China

*Master degree, majoring in clinical medicine*

09/2005 – 07/2010    Medical College of Southeast University, Nanjing, China

*Bachelor degree, majoring in clinical medicine*

**PUBLICATIONS**

**Zhi Zuo, Tatiana Syrovets, Felicitas Genze, Alireza Abaei, Genshan Ma, Thomas Simmet, Volker Rasche.** High-resolution MRI analysis of breast cancer xenograft on the chick chorioallantoic membrane. NMR Biomed. 28, 440–447 (2015).

**Zhi Zuo, Tatiana Syrovets, Weina Liu, Ina Vernikouskaya, Felicitas Genze, Alireza Abaei, Yuzhou Wu, Genshan Ma, Tanja Weil, Thomas Simmet, Volker Rasche.** Assessment of bio-distribution of Gd contrast agent in breast cancer xenografts on the CAM @ 11.7T. NMR Biomed. Submitted.

**ABSTRACTS**

**Zhi Zuo, Tatiana Syrovets, Felicitas Genze, Alireza Abaei, Genshan Ma, Thomas Simmet, Volker Rasche.** High-resolution MRI analysis of breast cancer xenografts on the CAM @ 11.7T, 2015 (Educational Stipend awarded)